SOME PROBLEMS OF INTEGRAL GEOMETRY IN ADVANCED IMAGING

by

RIM GOUIA

Presented to the Faculty of the Graduate School of

The University of Texas at Arlington in Partial Fulfillment

of the Requirements

for the Degree of

DOCTOR OF PHILOSOPHY

THE UNIVERSITY OF TEXAS AT ARLINGTON

May 2011

In the name of GOD, Most Gracious, Most Merciful

ACKNOWLEDGEMENTS

First of all, I am grateful to my supervising professor Dr. Gaik Ambartsoumian for his constant support, his thoughtful leadership and invaluable advice. His patience, seriousness, and commitment have helped me grow academically and face challenging problems with confidence. These words are too short of truly thanking his understanding and guidance. I will forever be in debt to him.

I thank my academic advisors Dr. Su, Dr. Liao, Dr. Aktosun, Dr. Lewis, and Dr. Kojouharov for their interest in my research and for their kind agreement to serve in my dissertation committee. I also thank my academic advisors, Dr. Grantcharov, and Dr. Burghduff for taking the time to write my recommendation letters and for contributing to my professional success.

I acknowledge all the faculty and staff at the Department of Mathematics at the University of Texas at Arlington, who helped me to finish my Ph.D. and all the friends that I met as a graduate student, especially the following people: Dr. Zhu, Dr. Hawkins, Dr. Jorgensen, Dr. Shipman, Dr. Korzeniowski, Dr. Gornet, Dr. Liu, Dr. Pankavich, Dr. Vancliff, Mr. Smith, Dr. Topsakal, Vishti, Kim, Cecelia, Shelley, Beth, Manizheh, Padmini, Alicia, Jennifer, Kristen, Angela and Julie... (I am missing many more).

I am grateful to all the teachers who taught me during my years in school in Tunisia and France. I owe special thanks to those special math professors Dr. Boukrisha, Mr. Latrach, and Dr. Colin who inspired me through my high school and undergraduate studies.

I gratefully acknowledge financial support from the following bodies: The University of Texas at Arlington, Department of Defense Medical Research Program, and Norman Hackerman Advanced Research Program.

Last and definitely not the least, none of this would have been close to reality if not for my graceful parents Dr. Houda Abdellah and Dr. Ridha Gouia and their unconditional love and support. They inspired every moment of my life from the baby steps to dreams and aspirations I carry in my heart. I will never be able to return their favors on me. I can only pray for their blessing. I forever indebted to my husband Samir and my beloved son Mohamed-Aziz for their unconditional support and love, no matter what the circumstances were.

March 30, 2011

ABSTRACT

SOME PROBLEMS OF INTEGRAL GEOMETRY IN ADVANCED IMAGING

Rim Gouia, Ph.D.

The University of Texas at Arlington, 2011

Supervising Professor: Dr. Ambartsoumian

During the past decade, our society has become dependent on advanced mathematics for many of our daily needs. Mathematics is at the heart of the 21st century technologies and more specifically the emerging imaging technologies from thermoacoustic tomography (TAT) and ultrasound computed tomography (UCT) to nondestructive testing (NDT). All of these applications reconstruct the internal structure of an object from external measurements without damaging the entity under investigation. The basic mathematical idea common to such reconstruction problems is often based upon Radon integral transform.

The Radon integral transform $R: f \mapsto Rf$ puts into correspondence to a given function f its integrals over certain subsets. In this work, we focus on the situation when the subsets are circles. The major problems related to this transform are the existence and uniqueness of its inversion, inversion formulas, and the range description of the transform. When Rf is known for circles of all possible radii, there are well developed theories addressing most of the questions mentioned above. However, many of these questions are still open when Rf is available for only a part of all possible radii.

The aim of my dissertation is to derive some new results about the existence and uniqueness of the representation of a function by its circular Radon transform

with radially partial data for both interior and exterior problems. The presented new results open new frontiers in the field of medical imaging such as intravascular ultrasound (IVUS) and transrectal ultrasound (TRUS).

TABLE OF CONTENTS

LIST OF FIGURES

LIST OF TABLES

CHAPTER 1

INTRODUCTION

During the past decade, our society has become dependent on advanced mathematics for many of our daily needs. Mathematics is at the heart of the 21st century technologies and more specifically the emerging imaging technologies from thermoacoustic tomography (TAT) and ultrasound computed tomography (UCT) to nondestructive testing (NDT). All of these applications reconstruct the internal structure of an object from external measurements without damaging the entity under investigation. Very often the basic mathematical idea common to such reconstruction problems is based upon integral geometry.

In accordance with the terminology used by I. Gelfand and G. Shilov in [31], integral geometry is the branch of geometrical analysis that analyzes integral transforms of geometrical nature. More specifically, integral geometry is dealing with properties of functions that can be determined by transforms integrating the function over subsets. This type of transforms are named Radon integral transforms after the Austrian mathematician, Johann Radon (1887-1956), who studied the transform that integrates functions of two independent variables over all lines in the plane for pure mathematical reasons. In 1963, the physicist Allan M. Cormack reinvented the classical Radon transform and supplanted it as the mathematical model of X-ray computed tomography (CT) in which the internal structure of an object can be determined by its integrals over all lines in the plane. Based upon Cormack's work, the engineer Godfrey Hounsfield invented the CT that revolutionized the field of medical imaging and resulted in the 1979 Nobel Prize in Physiology and Medicine.

The success of this imaging method and the tremendous improvement in the computing capabilities boosted the connection between integral geometry and medical

imaging as well as other fields of imaging such as non-destructive testing, geophysics, radar and sonar. Indeed, integral geometry is used in medicine to visualize internal organs, in non-destructive testing to evaluate the thickness of objects and flaws in materials, in geophysics to explore oil and gas, and in remote sensing to detect objects and monitor risk areas.

In the next chapter, we give a brief survey of some of the major imaging applications that deal with reconstructing the internal structure of an object without causing damage to it. The basic mathematical idea common to such reconstruction problems is based upon integral transforms of Radon type. In chapter 3, some of these transforms are defined and studied from a theoretical point of view. We first define the classical Radon transform, then we generalize it to the spherical and the elliptical Radon transforms, which are more relevant tools in the imaging applications that we consider. In chapter 4, we discuss some of the main mathematical problems that typically arise while determining a function from its Radon transforms. We start by a quick summary of the results regarding the inversion of the classical Radon transform in $\mathbb{R}^2$. We provide some of the important techniques that are used in the case of main interest. Then we intensively study the inversion of the spherical Radon transform in $\mathbb{R}^2$ and in $\mathbb{R}^n$ for $n > 2$. Once we show some of the techniques of reconstruction using complete data of the spherical Radon transform, we then concentrate, in chapter 5, on the question of representing a function by its circular Radon transform with partial data. We focus on the case of transforms integrating functions of two independent variables along circles, and present a new inversion formula when the Radon transform is known for only a part of all possible radii, for both interior and exterior problems. Finally in chapter 6, an approximate backprojection algorithm is developed to recover a 2D function from its integrals over a family of ellipses. We

also present the results of the numerical simulation where the center of the ellipses is rotating around the origin.

CHAPTER 2

MAJOR FIELDS OF APPLICATION

There are numerous imaging applications that deal with reconstructing the internal structure of an object without causing damage to it. The basic mathematical idea common to many of such reconstruction problems is based upon integral geometry. In this chapter, we describe some of the typical applications that use integral geometry in their mathematical models.

2.1 X-ray computed tomography

X-ray computed tomography, abbreviated to CAT or CT, consists of a tube emitting a thin collimated beam of X-rays that penetrates the object under investigation, and of a detector, which is recording the intensity loss of the transmitted X-rays. By rotating the source and the detector in the same plane around the patient, it is possible to obtain a set of projections. This collected data is processed by a computer to produce an image of the internal structure of the object from the external

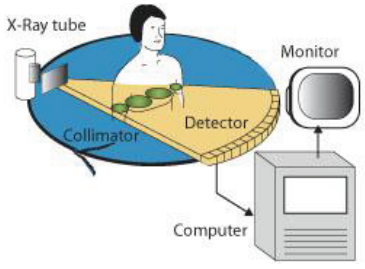

http://www.drkellysmiles.com/NewTechnology.aspx

Figure 2.1. Principle of measurement of an X-ray computed tomography.

measurements. Invented by the engineer Godfrey Hounsfield and the physicist Allan Cormack in 1972, the CT revolutionized the field of medical imaging.

As X-rays travel along a line L from the X-ray source through the object to an X-ray detector, the energy is attenuated by the material on the line L. The attenuation coefficient $f(x)$ at the point x is the function that quantifies the tendency of an object to absorb X-rays. Assuming all X-rays are sent in the same plane $x = (x_1, x_2)$ is a two dimensional variable, and $f(x)$ represents an image of a cross-sectional slice of the body. Let $I_{(\text{source})}$ and $I_{(\text{detector})}$ are, respectively, denote the initial intensity of the beam and the intensity of the beam after passing the object. So the relative intensity loss when the X-rays traverse a distance $\triangle x$ is

$$\triangle I/I = -f(x) \triangle x.$$

By integrating from the source to the detector, we get the following integral transform

$$\ln \left[\frac{I_{(\text{source})}}{I_{(\text{detector})}} \right] = \int_L f(x) dx.$$

Since $I_{(\text{source})}$ and $I_{(\text{detector})}$ are measured, the line integrals of the attenuation coefficient f along each of the lines L are known and can be used to reconstruct f. It is this mathematical model upon which CT is used in medicine as well as in industry for internal inspection of components, flaw detection, failure analysis, and metrology. An in-depth discussion of the X-ray tomography can be found in [23, 25, 33].

2.2 Ultrasound tomography

Ultrasound tomography is very similar to X-ray tomography. In both cases, we are trying to reconstruct a cross-sectional image from the recorded data. However, when using ultrasound as a form of energy to illuminate the object, the transmitted signal is almost immeasurable as most of the the energy is reflected by density contrasts. Hence, the reconstruction is done using reflected signals (Figure 2.2).

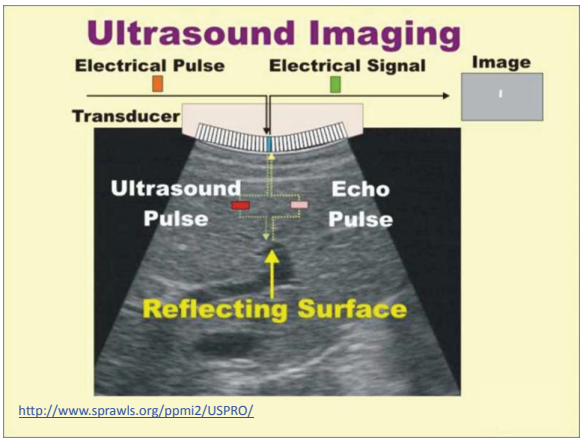

Figure 2.2. The basic ultrasound imaging process.

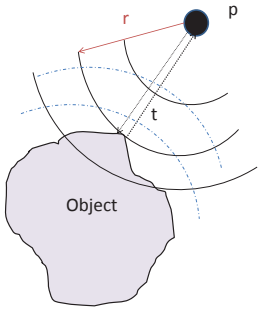

Figure 2.3. The receiver coincides with the source.

The transducer placed at the edge of the body works in dual modes first as an emitter of sound waves, and then as a receiver, registering the reflection of ultrasound waves from the inclusions inside the body.

Assuming that (1) the pulse radiates isotropically in the form of expanding spherical waves, (2) the speed of sound propagation c is constant, (3) the receiver coincides with the source, and (4) the medium is weakly reflecting (here by weakly reflecting we mean that multiple reflections are ignored), the signals registered by a transducer at any moment of time t would be generated by inclusions lying on a

sphere of radius $r = ct/2$ (Figure 2.3) centered at the transducer location. In other words, the recorded data $g(p, r)$ is surface integrals over spheres $S(p, r)$ centered at the transducer locations p and of radius $r = ct/2$.

$$g(p, r) = \int_{S(p,r)} f(x)\, d\sigma.$$

By moving the transducer over a hyperplane or on a hypersphere around the object, it is possible to collect enough data to reconstruct the image of the entire object.

One needs to notice that in the case of the omission of one of these assumptions, the spherical integral geometry is no longer valid. For example, in a bistatic setup where the receiver and the source are no longer collocated, the collected data $g(r, s, t)$ is the integrals of the image function f along ellipses with foci the source s and the receiver r, and semi-major axis $t/2$ (see e.g. [39, 40]). This leads us to another integral transform

$$g(r, s, t) = \int_{E(r,s,t)} f(x)\, d\sigma.$$

To reduce the imaging geometry to two dimensions, we consider a transducer that generates a cylindrical wavefront instead of spherical wavefront. This can be achieved in practice by using a transducer that focuses in the axial direction and reduce the thickness of the lateral direction.

The most well known application of ultrasound tomography is its use in medical imaging to produce pictures of the internal structure of the human body. Moreover, there are a vast number of other applications including radar imaging (Figure 2.5) and sonar (see e.g. [16, 18, 38]) for the case where the receiver coincides with the

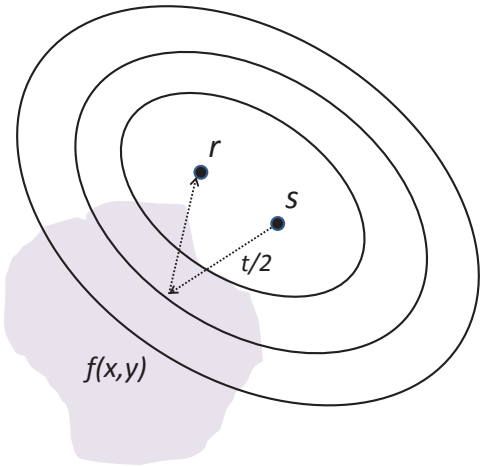

Figure 2.4. The receiver and the source are no longer collocated.

source, and geophysics (Figure 2.6) for the case where the receiver and the source are not collocated.

2.3 Thermoacoustic/photoacoustic tomography

Thermoacoustic tomography (TAT) and photoacoustic (PAT) tomography are two emerging medical imaging modalities based on a physical effect originally discovered by Alexander Graham Bell in 1880. These novel hybrid methods combine the advantages of optical absorption contrast with ultrasonic spatial resolution (see [3, 34] for a comprehensive survey on mathematical problems in TAT and PAT).

The part of the human body being imaged is exposed to a short pulse of electromagnetic (EM) radiation (radio-frequency (RF) waves in TAT, and lasers in PAT). A portion of this radiation is absorbed in the body, heating up the tissue, and causing

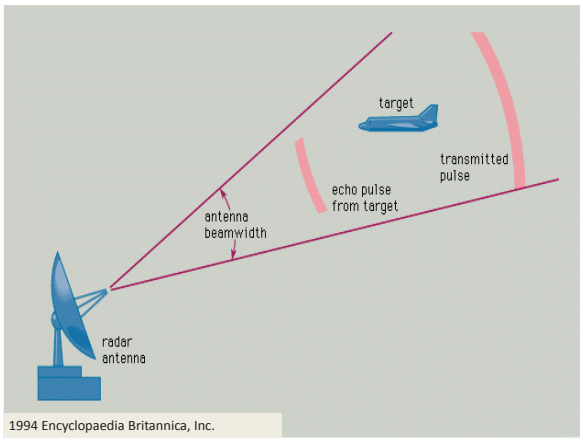

Figure 2.5. Radar.

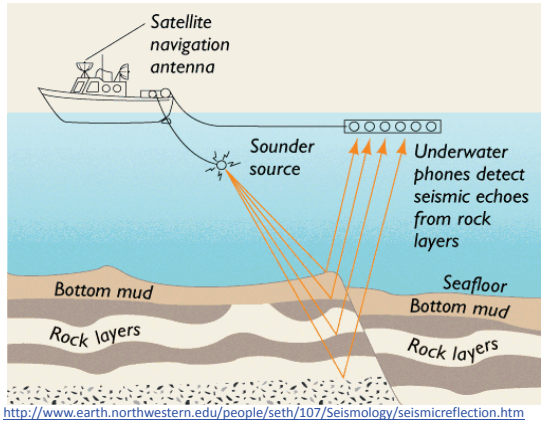

Figure 2.6. Geophysics.

thermal expansion, which in turn generates pressure waves (an ultrasound signal) traveling through the body. These acoustic waves are measured by multiple transducers placed along the body. Then the collected data is processed to generate an image of the heat absorption function inside the body. The premise here is that there exists a strong contrast in the amount of absorbed EM energy between different types of tissues. For example cancerous cells absorb several times more energy than the healthy ones, hence recovery of the RF absorption function inside the body can help

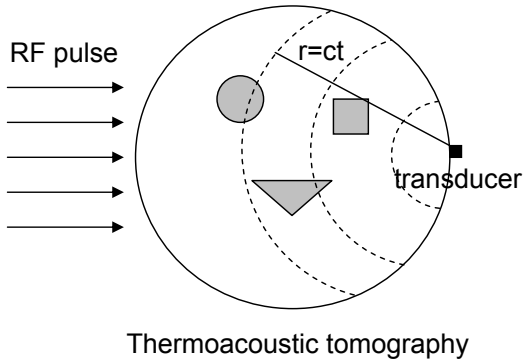

Figure 2.7. A sketch of TAT/PAT.

both to diagnose and to locate cancer. Figure 2.7 illustrates the process by which TAT and PAT are generated.

Since sound waves have very weak contrast in the tissue, we can simplify the model assuming the sound speed c to be constant in the body. Under this assumption the signals registered by a transducer at any moment of time t would be generated by inclusions lying on a sphere of radius $r = ct$ centered at the transducer location. Thus the problem of image reconstruction in TAT and PAT is equivalent to the recovery of the RF absorption function (the image to be reconstructed) from its integrals along spheres centered at available transducer locations. To reduce the imaging process to two dimensions, we limit the detection to circular signals by focusing the microphone to the plane.

In this chapter, we have concentrated on some of the imaging applications in which integral geometry has been found useful. Although a lot of advances have been made in this field, there are still cases (e.g. incomplete data problems) when the desired resolution and contrast are not yet achieved. Therefore, there remains a compelling need for the advancement of integral geometry and more specifically of

the knowledge about integral transforms of Radon type. That is what motivates our study in the upcoming chapters.

CHAPTER 3

SOME RADON INTEGRAL TRANSFORMS

The problem of image reconstruction in all the applications presented in the previous chapter, is equivalent to the recovery of the unknown function f from the collection of measured data Rf which is the set of integrals of the function f over certain hypersurfaces. In this chapter, we present a mathematical description of the relations between f and Rf for various choices of integration subsets. These relations are named Radon integral transforms after the Austrian mathematician J. Radon (1887-1956), who studied the transform that integrates functions of two and three independent variables respectively over lines and hyperplanes. It was later generalized to higher dimensions, and extended to broader geometries in the context of integral geometry introduced by I. Gelfand and G. Shilov in [31].

Next, we define and study some of the generalized Radon integral transforms from a theoretical point of view. First, we define the integral transform along the simplest path which is the straight line, called the classical Radon transform [1]. Then we generalize it to the spherical and the elliptical Radon transforms which are more relevant tools in advanced imaging that we consider.

3.1 Classical Radon transform

- Two dimensions

The classical Radon transform in 2D maps a function on $\mathbb{R}^2$ into the set of its integrals over straight lines in the plane. Let $(x,\ y)$ designate coordinates of points in the plane and $f(x, y)$ be an arbitrary function defined on some domain D $\subset \mathbb{R}^2$. The classical

[1] While this is not the topic of our research, some of the methods and approaches developed for the study of these transforms prove to be useful for our models later.

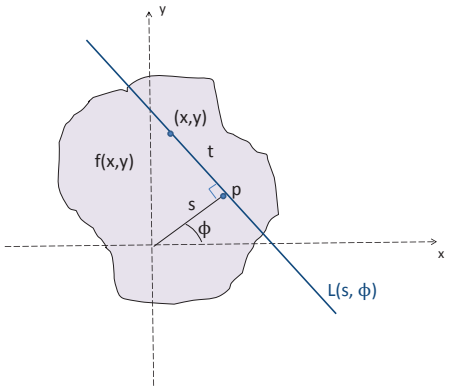

Figure 3.1. Geometric setup of integration along the line $L(s, \phi)$.

Radon transform Rf of f is a function defined on the space of straight lines L in $\mathbb{R}^2$ by the integral of f along each such line:

$$Rf(L) = \int_L f(x, y)\, dl,$$

where dl is the arc length element along L. The lines in the plane can be parameterized by 2 variables (s, ϕ), s.t. $L(s, \phi)$ denotes the line at oriented distance s from the origin and perpendicular to the vector $(\cos(\phi), \sin(\phi))$ (see Figure 3.1). Any point (x, y) along $L(s, \phi)$ can be parameterized by:

$$x(t) = s\cos\phi - t\sin\phi,$$

$$y(t) = s\sin\phi + t\cos\phi,$$

where the parameter $t \in (-\infty, \infty)$ is the signed distance measured from p to the point (x, y) on L (see Figure 3.1). The classical Radon transform can be expressed in these coordinates by

$$Rf(s, \phi) = \int_{-\infty}^{\infty} f(s\cos\phi - t\sin\phi, s\sin\phi + t\cos\phi)\, dt.$$

Alternative notation using the one-dimensional Dirac δ function is

$$Rf(s,\phi) = \int_{-\infty}^{\infty}\int_{-\infty}^{\infty} f(x,y)\,\delta(x\cos\phi + y\sin\phi - s)\,dx\,dy.$$

Note that Rf is an even function in the sense that

$$Rf(s,\phi) = Rf(-s,-\phi). \tag{3.1}$$

- Higher dimensions

More generally, in the n-dimensional space $\mathbb{R}^n$, the classical Radon transform maps a function on $\mathbb{R}^n$ into the set of its integrals over hyperplanes. Points in $\mathbb{R}^n$ are denoted by single letters $x = (x_1, x_2, \cdots, x_n)$ and functions defined on $\mathbb{R}^n$ by $f(x) = f(x_1, x_2, \cdots, x_n)$. The unit sphere in $\mathbb{R}^n$ is denoted by S^{n-1}. Let $H(s,\phi) = \{s \in \mathbb{R} : x \cdot \phi = s\}$ be the hyperplane orthogonal to $\phi \in S^{n-1}$ with oriented distance s from the origin. Using these notations, the classical Radon transform of f is defined by

$$Rf(s,\phi) = \int_{H(s,\phi)} f(x)\,dx.$$

Alternative notation is

$$Rf(s,\phi) = \int_{x\cdot\,\phi=s} f(x)\,dx.$$

We can also generalize the classical Radon transform by integrating over k-dimensional subspaces of $\mathbb{R}^n$; see, e.g. [32]. The ray transform is the most common case of this generalization, and is obtained by integrating functions over straight lines in $\mathbb{R}^n$. Thus for $n = 2$, the classical Radon transform and the ray transform differ only in the notation.

As previously explained, a simple imaging modality using the classical Radon transform is the X-ray tomography that consists of line integrals of the attenuation coefficient along all lines in the plane. A more precise definition of X-ray tomography can be found in chapter 2.

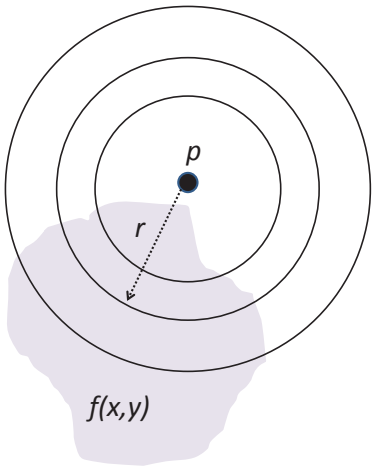

Figure 3.2. Geometric setup of integration along the circle $C(p, r)$.

3.2 Spherical Radon transform (SRT)

One can generalize the classical Radon transform to the spherical Radon transform for functions defined on $\mathbb{R}^2$, then on $\mathbb{R}^n$ as follows.

- Two dimensions

As the circle is the simplest curve in the plane next to the straight line, by analogy with the classical Radon transform, we define the circular Radon transform (CRT) of a function to be the path integral of the function along a circle of radius r and centered at the point $p \in \mathbb{R}^2$.

Let $f(x, y)$ be a continuous function on $\mathbb{R}^2$, then the CRT can be written as

$$Rf(p, r) = \int_{C(p,r)} f(x, y)\, dl,$$

where dl is the arc length element on the circle $C(p, r)$ of radius r and centered at $p \in \mathbb{R}^2$. Alternative notation using the one-dimensional Dirac δ function is

$$Rf(p, r) = \int_{-\infty}^{\infty} \int_{-\infty}^{\infty} f(x, y)\, \delta(r - \sqrt{x^2 + y^2})\, dx\, dy.$$

Remark: Although a lot of problems related to these Radon integral transforms have direct applications to mathematical models of modern technologies, some of them are investigated for pure theoretical reasons as they raise interesting and challenging mathematical questions.

- Extension to higher dimensions

More generally, in the n-dimensional space $\mathbb{R}^n$, we define the spherical Radon transform of a function to be the surface integral of the function along a hypersphere of radius r and centered at the point $p \in \mathbb{R}^n$. Let $f(x)$ be a continuous function on $\mathbb{R}^n$, then the spherical Radon transform of f can be written as

$$Rf(p,r) = \int_{|x-p|=r} f(x)\, d\sigma,$$

where $d\sigma$ is the area element on the sphere $|x-p| = r$ centered at $p \in \mathbb{R}^n$.

As mentioned before, the spherical Radon transform is commonly used in the reconstruction procedure adopted in ultrasound tomography. Indeed, under certain physical assumptions (1) the pulse radiates isotropically in the form of expanding spherical waves, (2) the speed of sound propagation c is constant, and (3) the receiver coincides with the source the problem of image reconstruction in ultrasound tomography is equivalent to the recovery of the image function f from Rf data along spheres centered at available transducer locations. Chapter 2 provides a more detailed description of ultrasound tomography and its imaging technique.

As mentioned before, in the case of the omission of one of these assumptions, the collected data Rf is the integrals of the image function f along ellipses with foci the source and the receiver locations. This leads us to the next section on the study of the elliptical Radon transform.

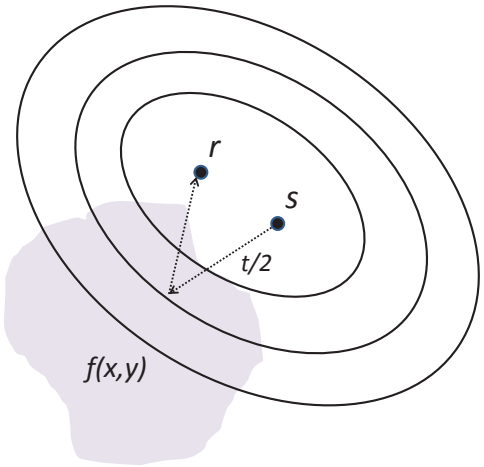

Figure 3.3. Geometric setup of integration along the ellipse $E(r, s, t)$.

3.3 Elliptical Radon transform (ERT)

We define the elliptical Radon transform of a function to be the path integral of the function along an ellipsoid of rotation with semi-major axis $t/2$ and foci $r, s \in \mathbb{R}^n$ (see e.g. [39, 40]).

- Two dimensions

Let $f(x, y)$ be a continuous function on $\mathbb{R}^2$, then the elliptical Radon transform can be written as

$$Rf(r, s, t) = \int_{E(r,s,t)} f(x, y)\, dl,$$

where dl is the arc length element on the ellipse $E(r, s, t)$. In this work, we only consider the 2D case, and possible future work can be done in 3D case.

Through this chapter, we presented some Radon integral transforms from a theoretical point of view and how they are related to data measured in applications. Therefore, the inverse problem that we consider is to reconstruct the unknown image

function f from the collection of measurements Rf. This reconstruction problem is equivalent to that of inverting the operator R defined as follows:

$$R: \quad f \longrightarrow Rf$$

$$\text{Unknown?} \longrightarrow \text{Data.}$$

Many mathematical problems naturally arise while studying the inversion question such as the existence and uniqueness of the inversion, inversion formulas and algorithms, the stability of these inversion algorithms, and the range of the Radon transforms (What conditions must the data satisfy?). These problems, with the exception of the stability and range descriptions, will be discussed intensively in the next chapter. For the detailed description and known results about stability and range descriptions, we refer the reader to papers [4, 10, 29, 56].

CHAPTER 4

MAIN MATHEMATICAL PROBLEMS AND KNOWN RESULTS

Among the major problems that naturally arise while studying the Radon integral transforms are the existence and uniqueness of their inversions, and inversion formulas and algorithms (e.g. [24, 42, 43]). These problems will be discussed throughout this chapter. We start by a quick summary of the results regarding the inversion of the classical Radon transform in $\mathbb{R}^2$ without providing details, as they are not our case of main interest [1]. Then we discuss in more details the inversion of the spherical Radon transform in $\mathbb{R}^2$ and in $\mathbb{R}^n$ for $n > 2$.

4.1 Classical Radon transform

Despite the discovery of the inversion formula of the classical Radon transform derived by J. Radon in his early work in 1917 for pure mathematical reasons, very little attention was given to implementing the inversion in a practical situation prior to the pioneering work of A. Cormack in [19] who won the Nobel Prize in Physiology and Medicine in 1979. Since then, this field has been investigated intensively. Today, there are well developed theories addressing the reconstruction problem. Several different approaches exist in the literature for inverting the classical Radon transform. The first one we introduce employs the harmonic decomposition technique used by A. Cormack. Then, we present the Fourier slice theorem, establishing a connection between the Fourier transform and the Radon transform. In the third section, we explore the most popular implementation of the Fourier slice theorem called filtered backprojection formula.

[1] While this is not the topic of our research, some of the methods and approaches developed for the study of these transforms prove to be useful for our models later.

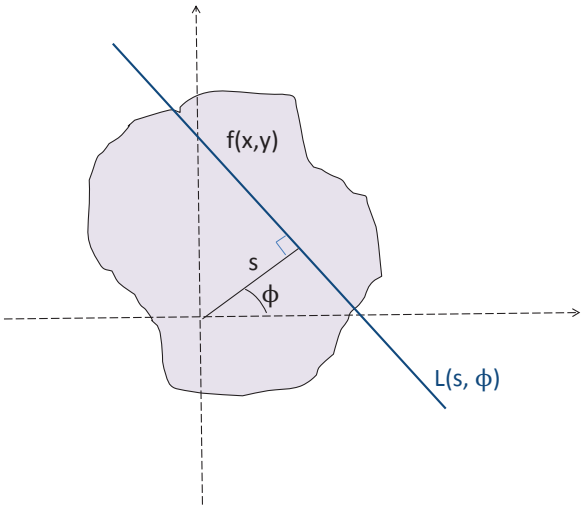

Figure 4.1. Coordinates to describe the line $L(s, \phi)$.

4.1.1 The Cormack method

Let $f(r, \theta)$ denote an unknown function supported inside the unit disc centered at the origin, where (r, θ) are polar coordinates measured from the center of the disc.

The classical Radon transform of f along the line L defined by the parameters (s, ϕ) is denoted by

$$g(s, \phi) = Rf(s, \phi) = \int_L f(r, \theta)\, dl. \tag{4.1}$$

Equation (4.1) is an integral equation in two variables but it may be reduced to a set of integral equations in one variable as follows. Since $f(r, \theta)$ and $g(s, \phi)$ are periodic with respect to the corresponding angular variables θ and ϕ, they can be expanded as Fourier series

$$f(r, \theta) = \sum_{n=-\infty}^{\infty} f_n(r)\, e^{in\theta}, \tag{4.2}$$

$$g(s, \phi) = \sum_{n=-\infty}^{\infty} g_n(s)\, e^{in\phi}, \tag{4.3}$$

where the Fourier coefficients $f_n(r)$ and $g_n(s)$ are computed by

$$f_n(r) = \frac{1}{2\pi}\int_0^{2\pi} f(r,\theta)\, e^{-in\theta} d\theta, \tag{4.4}$$

$$g_n(s) = \frac{1}{2\pi}\int_0^{2\pi} g(s,\phi)\, e^{-in\phi} d\phi. \tag{4.5}$$

The relation between $g_n(s)$ and $f_n(r)$ is given in [19] as

$$g_n(s) = 2\int_s^1 \frac{f_n(r)\; T_{|n|}(s/r)\, r\, dr}{(r^2 - s^2)^{\frac{1}{2}}}, \tag{4.6}$$

where $T_n(x)$ is the n-th order Tchebychev polynomial of the first kind (e.g. see [50]). It is easy to notice that by passing to the basis of complex exponentials, A. Cormack diagonalized the classical Radon transform, i.e. the n-th Fourier coefficient of g depends only on n-th Fourier coefficient of f. Equation (4.6) has the solution

$$f_n(r) = -\frac{1}{\pi}\frac{d}{dr}\int_r^1 \frac{g_n(s)\; T_{|n|}(s/r)\, s\, ds}{s(s^2 - r^2)^{\frac{1}{2}}}. \tag{4.7}$$

This formula is called Cormack's first inversion formula. Cormack's second inversion formula with imposed stability properties was derived later in [20]. Using the Zernicke polynomials (e.g. see [15]) ${R_n}^l(r)$, he derived the following reconstruction formula

$$f_n(r) = \sum_{l=0}^{\infty} (n + 2l + 1)\, {a_n}^l\, {R_n}^l(r),$$

where the ${a_n}^l$ are the coefficients appearing in the expansion

$$g_n(s) = 2\sum_{l=0}^{\infty} {a_n}^l \sin\left[(n + 2l + 1)\arccos(s)\right].$$

4.1.2 Fourier slice theorem

The Fourier transform and Radon transform are connected in a simple way. In imaging, this connection is called the Fourier slice theorem or equivalently the

projection-slice theorem. Following the same notation as in the previous section, let us define the one-dimensional Fourier transform of Rf

$$\widehat{Rf}(\rho,\phi) = \int_{-\infty}^{\infty} Rf(s,\phi)\, e^{-2\pi i\rho s}\, ds,$$

and the two-dimensional Fourier transform of f

$$F(u,v) = \int_{-\infty}^{\infty}\int_{-\infty}^{\infty} f(x,y)\, e^{-2\pi i(x\,u+y\,v)}\, dx\, dy. \tag{4.8}$$

According to the Fourier slice theorem, there is a connection between the two-dimensional Fourier transform of the function f and the one-dimensional Fourier transform of the Rf.

Let f be an absolutely integrable function in a domain $D \subset \mathbb{R}^2$. For any real number ρ and any angle ϕ, the Fourier slice theorem states

$$\widehat{Rf}(\rho,\phi) = F(\rho\,\cos\phi, \rho\,\sin\phi).$$

For an in-depth treatment of the theorem and its extension to n dimensions see [23].

4.1.3 Filtered backprojection method

Let us recall first the Fourier inversion of equation (4.8) in polar coordinates when f is an absolutely integrable function in a domain $D \subset \mathbb{R}^2$ and F is absolutely integrable

$$f(x,y) = \int_0^{2\pi}\int_0^{\infty} F(\rho\cos\phi, \rho\sin\phi)\, e^{2\pi i\,(x\rho\,\cos\phi + y\rho\,\sin\phi)}\, \rho\, d\rho\, d\phi. \tag{4.9}$$

Making use of the Fourier slice theorem, the equation (4.9) and the evenness property of Rf defined previously in the equation (3.1), we can establish the filtered backprojection (FBP) formula that states

$$f(x,y) = \int_0^{\pi}\int_{-\infty}^{\infty} \widehat{Rf}(\rho,\phi)\, e^{2\pi i\rho\,(x\cos\phi + y\sin\phi)}\, |\rho|\, d\rho\, d\phi.$$

The FBP formula can be understood as a two-step process:

1. The first inner integral is a filter applied to the Radon transform Rf. The filter represents a weighting of each projection in the frequency domain.
2. The outer integral is the backprojection of the filtered Radon transform.

To reconstruct the image at every point (x, y), the data is transformed to the frequency domain using one-dimensional Fourier transform, multiplied by the filter in the frequency domain, and then transformed back to the time domain using the one-dimensional inverse Fourier transform. The Radon transform data are referred to as the sinogram due to its characteristic sinusoidal shape. If the reconstruction were done without filtering, the form of the recovered image would be blurred. So in order to avoid artifacts and improve the quality of the reconstructed image, it is necessary to filter the data.

The next step involves a process known as backprojection which takes the filtered data and projects it back along the same lines from where the data was collected. So to compute the function at any given point (x, y), we average the filtered projections over all lines passing through that point. This FBP approach is useful for our discussion of the approximate inversion of the elliptical Radon transform developed in chapter 6.

Numerous other reconstruction schemes have been developed for inverting the Radon transform. For a survey see, e.g., [23, 25, 42]. Notice that all these inversion formulas uniquely determine the unknown function f from its classical Radon transform Rf. Hence, the uniqueness question is well known and answered. The same question when Rf is known only on a subset of the support of f is more complicated but well studied for the classical Radon transform (for more details, see [42]).

4.2 Spherical Radon transform

4.2.1 Uniqueness of reconstruction

Unlike the case of the classical Radon transform, the problem addressing the uniqueness of reconstruction is still not completely understood for the spherical Radon transform. In this section, we first formulate the problem of uniqueness of the spherical Radon transform and then present some of the recent mathematical results on uniqueness in $\mathbb{R}^2$ and $\mathbb{R}^n$ for $n > 2$.

4.2.1.1 Formulation of the problem

Let $f(x)$ be a continuous function on $\mathbb{R}^n$, the spherical Radon transform can be written as

$$Rf(p, r) = \int_{|x-p|=r} f(x)\, ds,$$

where ds is the surface area on the sphere $|x - p| = r$ centered at $p \in \mathbb{R}^n$. Without any restrictions on the set of centers p or radii r, $Rf(p, r)$ depends on $n + 1$ variables (one for the radius and n for the center's location). It is clear that the reconstruction of the function $f(x)$ of n variables from $Rf(p, r)$ is an overdetermined problem. It is reasonable to expect that one can still uniquely recover f from Rf after reducing the degrees of freedom of Rf by one. There are many different ways to reduce the dimensions of the Rf, e.g. by considering only the data coming from spheres of a certain fixed radius, spheres passing through a fixed point, spheres tangent to a hyperplane, spheres with centers located on a hypersurface, etc. All of these approaches lead to interesting mathematical problems and various research groups have done extensive amount of work on this subject. One can find good surveys and abundant lists of references to papers dedicated to these topics in [6, 9, 28, 30].

Motivated by several imaging applications described in chapter 2, we restrict the centers p to a set $\Gamma \subset \mathbb{R}^n$ while not imposing any conditions on the radii. So the first question that arises is whether knowing all the values of Rf on the set Γ uniquely determines the function f. Before addressing this problem, let us first define the notion of injectivity sets.

Definition 1. *Suppose* Γ *is a subset of* $\mathbb{R}^n$*. The spherical Radon transform is injective on* Γ *if for any* $f \in C_c(\mathbb{R}^n)$*, the condition* $Rf(p,r) = 0$ *for all* $r \geq 0$ *and for all* $p \in \Gamma$ *implies* $f \equiv 0$*. Such subsets* Γ *are called sets of injectivity for the spherical Radon transform on the class of compactly supported smooth functions.*

Here $C_c(\mathbb{R}^n)$ denotes the space of compactly supported continuous functions on $\mathbb{R}^n$. Using this definition, we can formulate the uniqueness question as follows: Which subsets Γ of $\mathbb{R}^n$ are injectivity sets of the spherical Radon transform?

4.2.1.2 Uniqueness of the circular Radon transform

The problem of describing the sets of injectivity of the circular Radon transform has been investigated intensively due to their connection to nodal sets for eigenfunctions of the Laplacian. The first work concerning non-injectivity sets was made in [37] by V. Lin and A. Pincus who considered the problem in relation to approximation theory. They proved that if Rf is not injective on Γ then Γ is contained in the zero set of a harmonic polynomial.

Their results were used in [6] by M. Agranovsky and T. Quinto who completely characterized the structure of the injectivity sets of a compactly supported function f when Rf is known along circles of all possible radii and centered on a given set. We will state their results but refer the reader to [6] for further details. Let us first introduce the following definition.

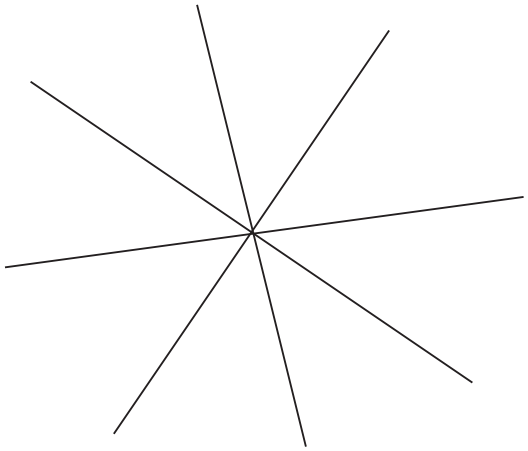

Figure 4.2. $L_k = \{te^{\frac{i\pi k}{N}} | -\infty < t < \infty\}$.

Definition 2. *For any positive integer N define $\sum_N$ to be the Coxeter system of N lines $L_0, ..., L_{N-1}$*

$$L_k = \{r\, e^{i\pi k/n} | k = 1, ..., N,\ r \in \mathbb{R}\}.$$

$\sum_N$ are N lines passing through the origin and forming equal angle π/N.

M. Agranovsky and T. Quinto characterized the injectivity sets in $\mathbb{R}^2$ in terms of Coxeter systems of lines.

Theorem 3. *A subset $\Gamma \subset \mathbb{R}^2$ is a set of injectivity for Rf on $\mathbb{R}^2$ if and only if Γ is not contained in any set of the form $Q(\sum_N) \cup Y$ for some N, for some rigid motion Q in the plane and some finite set Y.*

So the only subsets Γ of $\mathbb{R}^2$ which fail to be injectivity sets are either an empty set, a finite set or the union of a finite set and a Coxeter system of lines $\sum_N$. Any rigid motion Q preserves non-injectivity property, so $Q(\sum_N)$ is also a non-injectivity set.

For example in planar geometry, the line is a non-injectivity set, i.e. we can not recover f from the circular Radon transform Rf centered on a line. Indeed, if $f(x)$ is odd with respect to a line L, then if we integrate the function along circles centered on L, the measured data Rf is zero. So clearly the line, which is a subset of the $\sum_N$, is eliminated from the injectivity sets of the circular Radon transform. However, it is well known that functions that are even with respect to a line L can be reconstructed using the circular Radon transform centered on L (see [21]). It is also easy to see from this statement, that the functions supported only on one side of the line can be recovered uniquely (consider an even function which is equal to half of the previous function in the support).

4.2.1.3 Uniqueness of the spherical Radon transform

M. Agranovsky and T. Quinto in [6] conjectured the structure of the injectivity sets for the spherical Radon transform on the class of compactly supported function in higher dimensions.

Conjecture 4. *A set $\Gamma \subset \mathbb{R}^n$ is an injectivity set for the spherical Radon transform on $C_c(\mathbb{R}^n)$, if and only if it is not contained in any set of the form $Q(\sum_N) \cup Y$, where Q is a rigid motion of $\mathbb{R}^n$, $\sum_N$ is the zero set of a non-zero homogeneous harmonic polynomial, and Y is an algebraic subset in $\mathbb{R}^n$ of co-dimension at least 2.*

Unfortunately, the techniques of microlocal analysis and geometric properties of zero sets of harmonic polynomials used to prove the 2-dimensional conjecture, do not work well in dimensions higher than two or when the function is not compactly supported. So no proof of the conjecture is known at this time, as well as little is known about the non-injectivity sets for functions that are not compactly supported. A new alternative method based on a relation between the solutions of the wave equation and the spherical Radon transform has been investigated by M. Agranovsky,

C. Berenstein and P. Kuchment in [2]; D. Finch, S. Patch and Rakesh in [30]; and G. Ambartsoumian and P. Kuchment in [9]. This approach has led to new results promising possible progress to prove the n-dimensional conjecture.

We first mention the theorem in [2] of M. Agranovsky, C. Berenstein and P. Kuchment, who used PDE tools to study the injectivity of the spherical Radon transform when $f \in L^p(\mathbb{R}^n)$ and Rf is known for spheres of all possible radii centered at every point of the boundary of some domain.

Theorem 5. *The boundary Γ of any bounded domain in $\mathbb{R}^n$ is uniqueness set for $f \in L^p(\mathbb{R}^n)$ iff $p \leq \frac{2n}{n-1}$.*

In [30], D. Finch, S. Patch and Rakesh studied this uniqueness problem for smooth f supported in a bounded connected domain, proving the uniqueness of inversion using Rf from spheres centered on any open subset of the boundary of D and all possible radii $D \subset \mathbb{R}^n$.

Theorem 6. *Suppose D is a bounded open subset of $\mathbb{R}^n$, $n \geq 2$, with a smooth boundary S and the closure set $\bar{D}$ is strictly convex. Let Γ be any relatively open subset of S. If f is a smooth function on $\mathbb{R}^n$, supported in $\bar{D}$, and $Rf(p,r) = 0$ for all $p \in \Gamma$ and all $r \in [0, diam\, D]$ then $f \equiv 0$.*

Another result was reported in [9] by G. Ambartsoumian and P. Kuchment who reproved some known theorems using simpler methods and obtained further results on the injectivity of spherical Radon transform. They discovered same strong necessary conditions that any non-injectivity set has to satisfy, regardless of the dimensions of the problem and without requiring finite support of f. The formulation of the full result will require substantial space for extra definitions, so we present here just one corollary of the main theorem, referring the reader to [9] for more details.

Theorem 7. *Let Γ be a relatively open piece of C^1-hypersurface and $f \in C_c(\mathbb{R}^n)$ be such that $Rf(p,r) = 0$ for all $(p,r) \in \Gamma \times \mathbb{R}$. If there is a point $p_0 \in \Gamma$ such that the support of f lies strictly on one side of the tangent plane $T_{p_o}\Gamma$ to Γ at p_0, then $f \equiv 0$.*

Conclusion: We have presented some of the recent mathematical results on the uniqueness of the spherical Radon transform. In the case of compactly supported functions, non-uniqueness sets of the circular Radon transform are completely characterized. However, the uniqueness problem remains unresolved in dimensions higher than two, and even in dimension two it is not resolved for functions that are not compactly supported. Indeed, the problem is much harder to study without compactness of support.

Remark: All three theorems above guarantee the unique inversion of Rf in circular acquisition geometry when Rf is available for all possible radii (complete data). But the uniqueness question when Rf is available for only a part of all possible radii (partial data) is still an open problem. In the case of odd n, D. Finch, S. Patch and Rakesh proved in [30] the uniqueness of inversion from data with spheres centered at every point of the boundary and radii limited to $r < (\operatorname{diam} D)/2$. The proof of the latter result would not extend to even dimensions, since it was based on the solution properties of certain problems related to wave equation, that hold only in odd dimensions. In addition, M. Anastasio et al. showed in [11] that the 3D spherical Radon data for half of all possible radii is sufficient for unique reconstruction of the unknown function supported inside the sphere.

However, to the best of our knowledge no uniqueness result is known for even dimensions when only partial data is available. In our paper [7], we made progress in filling this gap in $\mathbb{R}^2$, by proving uniqueness for the circular Radon transform collected along all circles of radii $r < (\operatorname{diam} D)/2$. We also addressed another open problem of

uniqueness when the support of the unknown function extends outside of the circle. These new results are presented in details in the next chapter.

4.2.2 Reconstruction formulas

Many explicit inversion formulas have been derived from the spherical Radon transform centered on some simple geometries. The first studied geometry was the hyperplane in [14, 21, 26, 44]. As it has been mentioned in the previous section, there is no uniqueness in this case, only even functions can be reconstructed from the spherical Radon transform. Another geometry investigated in [47, 54] was the infinite cylinder in three-dimensional space. We do not provide details about the reconstruction formulas in these geometries as they are not our case of interest.

In this section, we confine our discussion to the spherical geometry as it is the most relevant acquisition to the imaging modalities described in the first chapter. We state some of the known methods to derive explicit inversion formulas from the spherical Radon transform centered on a sphere.

4.2.2.1 Fourier expansion methods

The first approach to tackle the problem of reconstructing a function supported in a disc D from its spherical Radon transform along circles centered on the boundary of D, was described by S. Norton [46] in his study of ultrasonic reflection tomography. He derived an inversion formula based on harmonic decompositions for the measured circular Radon transform and the 2D unknown function. This paper has been an inspiration to many subsequent works.

Throughout this section $f(r, \theta)$ denotes a two-dimensional function supported inside the disc $D(0, R)$, where (r, θ) are polar coordinates measured from the center of that disc, and $R > 0$ is a fixed number. The circular Radon transform Rf along a

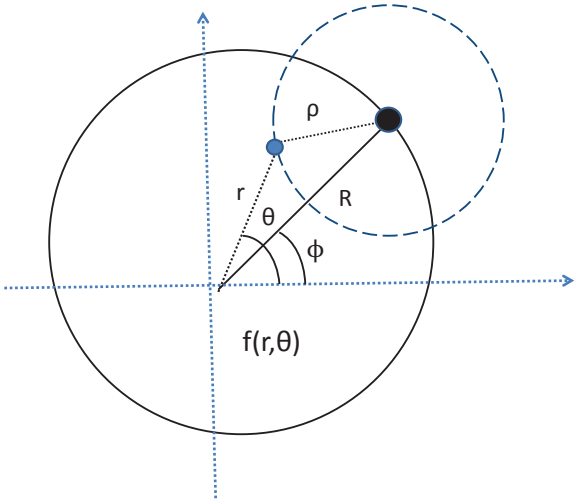

Figure 4.3. Circle geometry $C(\rho, \phi)$.

circle of radius ρ centered at a point with polar coordinates (R, ϕ) (see Figure 4.3) is denoted by

$$g(\rho, \phi) = Rf(\rho, \phi) = \int_{C(\rho,\phi)} f(r, \theta)\, ds. \tag{4.10}$$

Since $f(r, \theta)$ and $g(s, \phi)$ are periodic with respect to the corresponding angular variables θ and ϕ, they can be expanded as Fourier series

$$f(r, \theta) = \sum_{n=-\infty}^{\infty} f_n(r)\, e^{in\theta}, \tag{4.11}$$

$$g(\rho, \phi) = \sum_{n=-\infty}^{\infty} g_n(\rho)\, e^{in\phi}, \tag{4.12}$$

where the Fourier coefficients $f_n(r)$ and $g_n(\rho)$ are computed in (4.4) and (4.5).

The circular Radon transform as expressed by Eq.(4.10), can be written in terms of Dirac delta function

$$g(\rho, \phi) = \int_0^{\infty} r\, dr \int_0^{2\pi} d\theta\, f(r, \theta)\, \delta[\rho - (r^2 + R^2 - 2rR\cos(\phi - \theta))^{1/2}].$$

The solution to the problem is obtained by using the property of Dirac delta function

$$\delta(\beta - \rho) = \rho \int_0^\infty J_0(\beta z) J_0(\rho z) z \, dz,$$

and deriving a relation expressing the n-th Fourier coefficient $f_n(r)$ in terms of the n-th Fourier coefficient $g_n(\rho)$. In other words, the circular Radon transform is diagonalized by passing to the basis of complex exponentials. This is not surprising due to the rotation invariance of $g(\rho, \phi)$ in the circular geometry. As a result the problem breaks down to the following set of one-dimensional integral equations

$$g_n(\rho) = 2\pi\rho \int_0^\infty z J_0(\rho z) J_n(Rz) \mathcal{H}_n\{f_n(r)\} dz, \tag{4.13}$$

where $\mathcal{H}_n$ with $\mathcal{H}_n\{p(r)\}_z = \int_0^\infty p(r) J_n(rz) r dr$ is the n-th order Hankel transform and $J_n(r)$ are the Bessel functions of the first kind.

Using the fact that the Hankel transform is its own inverse, the coefficients $f_n(r)$ can be recovered by the following formula

$$f_n(r) = \mathcal{H}_n \left\{ \frac{1}{J_n(Rz)} \mathcal{H}_0 \left\{ \frac{g_n(\rho)}{2\pi\rho} \right\}_z \right\}_r. \tag{4.14}$$

The function $f(r, \theta)$ can now be reconstructed by inserting the $f_n(r)$ into the angular Fourier series (4.11). Notice this inversion formula requires a division of the Hankel transform by the Bessel functions that have infinitely many zeros. In the numerical implementation, these zeros would create instabilities. So recently, there have been new additions in this approach in [34] to avoid this instability problem by replacing the Bessel functions by Hankel functions $H_n^{(1)}$ which does not have zeros for any real values. Eq. (4.14) becomes

$$f_n(r) = \mathcal{H}_n \left\{ \frac{1}{H_n^{(1)}(Rz)} \int_0^{2R} g_n(\rho) H_0^{(1)}(\rho z) d\rho \right\}. \tag{4.15}$$

In a similar way, S. Norton and M. Linzer in [47] derived an inversion formula for the three-dimensional case involving a series expansion in spherical harmonics.

All these mentioned works assume that the object of interest is entirely surrounded by the circular aperture. They also require a complete knowledge of the circular Radon transforms $g(\rho, \phi)$ for all the values of ρ and ϕ. In fact, to be able to reconstruct the function f at any point (r, θ), all the values of $g(\rho, \phi)$ are essential.

4.2.2.2 Filtered backprojection methods

The filtered backprojection method is the most common technique in image reconstruction that requires the inversion of the spherical Radon transform. It transforms the data to the frequency domain, then filters in order to smooth out the noise, returns to the time domain and then applies a backprojection. The inversion formulas of filtered backprojection type do not involve series but are instead given as integrals. The first exact formulas of this type were proven in [30] by D. Finch, S. Patch and Rakesh in odd dimensions, and then extended recently to even dimensions in [27] by D. Finch, M. Haltmeier and Rakesh.

Let us start with some notations to state the explicit inversion formulas. For any integer $n > 1$, we assume that the unknown function $f(x)$ is supported inside the ball B of radius R in $\mathbb{R}^n$, which is centered at the origin. We also assume that the spherical Radon transform $Rf(p, r) = g(p, r)$ is known for all spheres of radius r centered at the point p on the spherical boundary S_R of the ball.

$$g(p, r) = \int_{|p-x|=r} f(x)\, d\sigma. \tag{4.16}$$

Let $\hat{C}^\infty(S_R \times [0, \infty))$ denote the class of smooth functions $g(p, t)$ which are zero to infinite order in t at $t = 0$. The operator $\mathcal{D}$ is defined as follows

$$\begin{aligned} \mathcal{D} : \hat{C}^{\infty}(S_R \times [0,\infty)) &\rightarrow \hat{C}^{\infty}(S_R \times [0,\infty)) \\ g(p,t) &\rightarrow \left(\frac{1}{2t}\frac{\partial}{\partial t}\right) g(p,t). \end{aligned}$$

It is also convenient to define $\mathcal{N}$

$$\begin{aligned} \mathcal{N} : C_0^{\infty}(\bar{B}) &\rightarrow \hat{C}^{\infty}(S_R \times [0,\infty)) \\ f(p,t) &\rightarrow t^{n-2} g(p,t), \end{aligned}$$

whose L^2-adjoint is $\mathcal{N}^*$, which is given as follows

$$\begin{aligned} \mathcal{N}^* : \hat{C}^{\infty}(S_R \times [0,\infty)) &\rightarrow C_0^{\infty}(\mathbb{R}^n) \\ F(x) &\rightarrow \frac{1}{w_{n-1}} \int_{|p|=R} \frac{F(p,|p-x|)}{|p-x|}\, ds, \end{aligned}$$

where w_{n-1} surface area of the unit sphere. Since the inversion formulas are different for the odd and even dimensions, we state them separately.

- *Inversion for odd n*

Theorem 8. *If n is odd and $f \in C_0^{\infty}(\bar{B})$ then for all $x \in B$, the following reconstruction formulas hold true*

$$f(x) = \frac{c_n}{R} \triangle_x \left(\mathcal{N}^* t \mathcal{D}^{n-3} t^{n-4} g\right)(p\,,t),$$

where $\triangle_x$ is the Laplacian with respect to the first variable and

$$c_n = \frac{(-1)^{(n-1)/2}\pi}{2\Gamma(n/2)^2}.$$

In the case $n = 3$, it may be written

$$f(x) = -\frac{1}{2\pi\, R} \triangle_x \int_{|p|=R} \frac{1}{|x-p|} g(p,|x-p|) ds.$$

The proof of the three-dimensional theorem is based on an explicit computation of the integral. However, the n-dimensional theorems were deduced by the use of spherical harmonic expansions.

- *Inversion for even n*

Theorem 9. *If n is even and $f \in C_0^\infty(\bar{B})$ then for all $x \in B$*

$$f(x) = \frac{2}{c_n R} \int_{|p|=R} \int_0^{2R} \left(log|t^2 - |x-p|^2| \right) \left((t\mathcal{D}^{n-1} t^{n-1} \partial_t g)(p\,,t) \right) \, dt\, ds,$$

where

$$c_n = (-1)^{n-2/2} 2\,[(n-2)/2)!]\,\pi^{n/2}.$$

In the case $n = 2$, it may be written

$$f(x) = \frac{1}{2\pi R} \int_{|p|=R} \int_0^{2R} log|t^2 - |x-p|^2| (\partial_t\, t\, \partial_t\, g)(p\,,t)\, dt\, ds. \tag{4.17}$$

The theorem was proved in [27] using a spherical harmonic expansion and the trace of the solution of the wave equation in even dimensions.

Another interesting inversion formula for the spherical geometry was presented by M. Xu and L. Wang in [54] called the universal backprojection algorithm which offers exact reconstruction for three common geometries: planar, spherical and cylindrical surfaces.

In [35], L. Kunyansky presented an inversion formula for any arbitrary dimensions $n > 1$, similar to the result of M. Xu and L. Wang in [54].

Remark: We have summarized some of the recent mathematical results for the problem of recovering a function from the spherical Radon transform. All presented formulas assume that a complete data set is available, i.e. the values of the spherical Radon transforms $g(p, r)$ are known for all the values of p and r. For example in the equation (4.17), a complete knowledge of $g(p, r)$ is needed to reconstruct the function f at any point x. So how to recover f if the experimental implementation does not provide the complete data set?

The hypothesis that all the values of the spherical Radon transform are known, is not always possible in imaging applications. For example, in some cases, because some regions of the object to be imaged strongly attenuate the signal, only partial data is available. In [12], M. Anastasio and his collaborators showed that using a partial data in Norton's formula [46] ($r \leq (\operatorname{diam} D)/2$) instead of the complete data ($r \leq \operatorname{diam} D$), results in severe image artifacts. Clearly, there is a significant need for a new reconstruction formula using partial data.

In our paper [7], we made progress in filling this gap by deriving new inversion formulas for the circular Radon transform collected along all circles of radii $r \leq r_0$ for $\forall\, r_0 < (\operatorname{diam} D)/2$. These new results are presented in details in the next chapter.

CHAPTER 5

RECONSTRUCTION FROM PARTIAL DATA OF SRT[1]

After we have shown some of the techniques of reconstructing f using complete data of the spherical Radon transform Rf, we now concentrate on the question of representing a function by its circular Radon transform with partial data. In this chapter, we present our new results about the existence and uniqueness of such representations, and a new inversion formula in the case of the circular acquisition geometry for both interior and exterior problems. The results are not only interesting as original mathematical discoveries, but can also be useful for many applications, e.g. in medical imaging.

5.1 Interior problem

Throughout this section $f(r,\theta)$ denotes an unknown function supported inside the disc of radius R, where (r,θ) are polar coordinates measured from the center of that disc, and $R > 0$ is a fixed number. The circular Radon transform of f along a circle of radius ρ centered at a point with polar coordinates (R,ϕ) (see Figure 5.1) is denoted by

$$g(\rho,\phi) = Rf(\rho,\phi) = \int_{C(\rho,\phi)} f(r,\theta)\, d\sigma. \tag{5.1}$$

The Fourier series generated by $f(r,\theta)$ and $g(\rho,\phi)$ with respect to corresponding angular variables are denoted by

$$f(r,\theta) = \sum_{n=-\infty}^{\infty} f_n(r)\, e^{in\theta}, \tag{5.2}$$

$$g(\rho,\phi) = \sum_{n=-\infty}^{\infty} g_n(\rho)\, e^{in\phi}, \tag{5.3}$$

where the Fourier coefficients $f_n(r)$ and $g_n(\rho)$ are computed in (4.4) and (4.5).

[1] This chapter is mainly based on the paper [7].

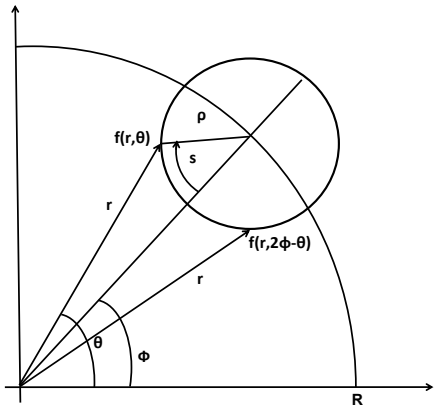

Figure 5.1. Geometric setup of integration along the circle $C(\rho, \phi)$.

We show that the function f can be uniquely recovered from Radon data with only part of all possible radii, and then provide a reconstruction formula.

5.1.1 Uniqueness of reconstruction

Theorem 10. *Let $f(r, \theta)$ be an unknown continuous function supported inside the annulus $A(\varepsilon, R) = \{(r, \theta) : r \in (\varepsilon, R),\, \theta \in [0, 2\pi]\}$, where $0 < \varepsilon < R$. If $Rf(\rho, \phi)$ is known for $\phi \in [0, 2\pi]$ and $\rho \in [0, R - \varepsilon]$, then $f(r, \theta)$ can be uniquely recovered in $A(\varepsilon, R)$.*

Proof. We use an approach similar to Cormack's inversion of the classical Radon transform [19]. Let us rewrite formula (5.1) by considering the contribution dg to $g(\rho, \phi)$ from two equal elements of arc ds of the circle $C(\rho, \phi)$. If the two elements of the arc are located symmetrically with respect to the polar radius of the center of integration circle (see Figure 5.1), then

$$dg = \sum_{n=-\infty}^{\infty} [f_n(r)\, e^{in\theta} + f_n(r)\, e^{in(2\phi-\theta)}]\, ds, \qquad 0 \le \phi \le \theta \le 2\pi$$

so we can write

$$g(\rho,\phi)=\int_{C^+(\rho,\phi)}\sum_{n=-\infty}^{\infty}\left[f_n(r)\,e^{in\theta}+f_n(r)\,e^{in(2\phi-\theta)}\right]ds,\qquad 0\le\phi\le\theta\le 2\pi,$$

where $C^+(\rho,\phi)$ denotes half of the circle $C(\rho,\phi)$ corresponding to $\theta\ge\phi$. Notice that $e^{in\theta}+e^{in(2\phi-\theta)}=2\,e^{in\phi}\cos[n(\theta-\phi)]$, and $s=\rho\arccos\left(\frac{\rho^2+R^2-r^2}{2\rho R}\right)$, hence

$$ds=\frac{rdr}{R\sqrt{1-\left(\frac{\rho^2+R^2-r^2}{2\rho R}\right)^2}}.$$

Exchanging the order of summation and integration and using these relations we get

$$g(\rho,\phi)=\sum_{n=-\infty}^{\infty}2\,e^{in\phi}\int_{R-\rho}^{R}\frac{f_n(r)\;r\cos[n(\theta-\phi)]}{R\sqrt{1-\left(\frac{\rho^2+R^2-r^2}{2\rho R}\right)^2}}\,dr.$$

Applying $\theta-\phi=\arccos\left(\frac{r^2+R^2-\rho^2}{2rR}\right)$, we obtain

$$g(\rho,\phi)=\sum_{n=-\infty}^{\infty}2\,e^{in\phi}\int_{R-\rho}^{R}\frac{f_n(r)\;r\cos\left[n\arccos\left(\frac{r^2+R^2-\rho^2}{2rR}\right)\right]}{R\sqrt{1-\left(\frac{\rho^2+R^2-r^2}{2\rho R}\right)^2}}\,dr. \tag{5.4}$$

Comparing equations (5.3) and (5.4) it is easy to notice that by passing to the basis of complex exponentials we diagonalized the circular Radon transform, i.e. the n-th Fourier coefficient of g depends only on n-th Fourier coefficient of f. This is not surprising, due to rotation invariance property of Rf in the circular geometry. As a result our problem breaks down to the following set of one-dimensional integral equations

$$g_n(\rho)=2\int_{R-\rho}^{R}\frac{f_n(r)\;r\;T_{|n|}\left(\frac{r^2+R^2-\rho^2}{2rR}\right)}{R\sqrt{1-\left(\frac{\rho^2+R^2-r^2}{2\rho R}\right)^2}}\,dr, \tag{5.5}$$

where $T_k(x)$ is the k-th order Chebyshev polynomial of the first kind (e.g. see [50]). Let us make a change of variables in the integral (5.5) by setting $u=R-r$. Then equation (5.5) becomes

$$g_n(\rho)=\int_0^{\rho}\frac{f_n(R-u)\,4\rho\,(R-u)\;T_{|n|}\left[\frac{(R-u)^2+R^2-\rho^2}{2R\,(R-u)}\right]}{\sqrt{\rho-u}\sqrt{(u+\rho)(2R+\rho-u)(2R-\rho-u)}}\,du, \tag{5.6}$$

which can be rewritten as

$$g_n(\rho) = \int_0^\rho \frac{F_n(u)\, K_n(\rho, u)}{\sqrt{\rho - u}}\, du, \tag{5.7}$$

where

$$F_n(u) = f_n(R - u), \tag{5.8}$$

$$K_n(\rho, u) = \frac{4\rho\,(R-u)\; T_{|n|}\left[\frac{(R-u)^2+R^2-\rho^2}{2R(R-u)}\right]}{\sqrt{(u+\rho)(2R+\rho-u)(2R-\rho-u)}}. \tag{5.9}$$

Equation (5.7) is a Volterra integral equation of the first kind with weakly singular kernel (e.g. see [49, 51]). Indeed, due to the assumptions on the support of f we know, that $F_n(u) \equiv 0$ for u close to R or 0. Therefore from formula (5.9) and the properties of Chebyshev polynomials, it follows that the kernel $K_n(\rho, u)$ is continuous in its arguments (and hence bounded) along with the first order partial derivatives on the support of F_n. To remove the singularity in the kernel of equation(5.7), we apply the standard method of kernel transformation [53]. Multiplying both sides of equation (5.7) by $\frac{1}{\sqrt{t-\rho}}\, d\rho$ and integrating from 0 to t we get

$$\int_0^t \frac{g_n(\rho)}{\sqrt{t-\rho}}\, d\rho = \int_0^t \int_0^\rho \frac{F_n(u) K_n(\rho, u)}{\sqrt{\rho - u}\sqrt{t-\rho}}\, du\, d\rho, \quad t > 0.$$

Changing the order of integration, we obtain

$$\int_0^t \frac{g_n(\rho)}{\sqrt{t-\rho}}\, d\rho = \int_0^t F_n(u)\; Q_n(t, u)\, du, \tag{5.10}$$

where

$$Q_n(t, u) = \int_u^t \frac{K_n(\rho, u)}{\sqrt{\rho - u}\sqrt{t-\rho}}\, d\rho.$$

The advantage of equation (5.10) in comparison to equation (5.7) is that the modified kernel $Q_n(t, u)$ is finite. Indeed, making a change of variables $\rho = u + (t-u)\, l$, $0 \le l \le 1$ in the last integral, we get

$$Q_n(t, u) = \int_0^1 \frac{K_n(u + (t-u)\, l, u)}{\sqrt{l}\,\sqrt{1-l}}\, dl. \tag{5.11}$$

Since K_n is bounded (say $|K_n| < M$), we obtain

$$|Q_n(t,u)| < M \int_0^1 \frac{dl}{\sqrt{l}\,\sqrt{1-l}} = M\pi.$$

In addition $Q_n(t,t) = \pi K_n(t,t) = \pi\sqrt{\dfrac{2t\,(R-t)}{R}} \neq 0$ on the support of F_n. Now we can easily modify equation (5.10) to a Volterra equation of second kind. Differentiating equation (5.10) with respect to t we get

$$\frac{d}{dt}\int_0^t \frac{g_n(\rho)}{\sqrt{t-\rho}}\,d\rho = \pi F_n(t)\; K_n(t,t) + \int_0^t F_n(u)\;\left[\frac{\partial}{\partial t}\int_u^t \frac{K_n(\rho,u)}{\sqrt{\rho-u}\sqrt{t-\rho}}\,d\rho\right]\,du.$$

Dividing both sides of the last equation by $\pi K_n(t,t)$ and denoting

$$G_n(t) = \frac{1}{\pi K_n(t,t)}\;\frac{d}{dt}\int_0^t \frac{g_n(\rho)}{\sqrt{t-\rho}}\,d\rho, \tag{5.12}$$

and

$$L_n(t,u) = \frac{1}{\pi K_n(t,t)}\;\frac{\partial}{\partial t}\int_u^t \frac{K_n(\rho,u)}{\sqrt{\rho-u}\sqrt{t-\rho}}\,d\rho. \tag{5.13}$$

We finally obtain a Volterra equation of second kind

$$G_n(t) = F_n(t) + \int_0^t F_n(u)\,L_n(t,u)\,du, \tag{5.14}$$

where the kernel $L_n(t,u)$ is continuous on the support of F_n. To see the continuity of L_n one can make a change of variables in equation (5.13)

$$\rho = t\cos^2\beta + u\sin^2\beta, \quad \beta \in [0,\pi/2],$$

and express L_n as

$$L_n(t,u) = \frac{2}{\pi\,K_n(t,t)}\;\frac{\partial}{\partial t}\int_0^{\pi/2} K_n(t\cos^2\beta + u\sin^2\beta, u)\,d\beta.$$

The Volterra equation of the second kind (5.14) has a unique solution, which finishes the proof of the theorem. $\square$

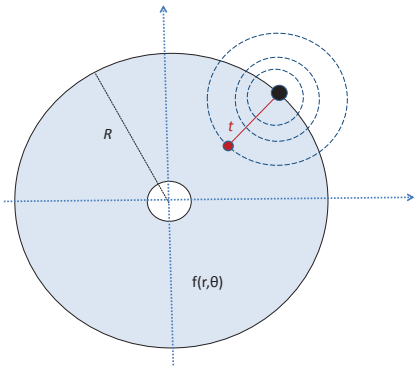

Figure 5.2. The interior problem.

5.1.2 Reconstruction formulas

Using the Picard process of successive approximations (e.g. see [51]) for the solution of Volterra equations of second kind one can immediately obtain the following

Corollary 11. *An exact solution of equation (5.14) is given by the formula*

$$F_n(t) = G_n(t) + \int_0^t H_n(t,u)\, G_n(u)\, du, \tag{5.15}$$

where the resolvent kernel $H_n(t,u)$ is given by the series of iterated kernels

$$H_n(t,u) = \sum_{i=1}^{\infty} (-1)^i L_{n,i}(t,u), \tag{5.16}$$

defined by

$$L_{n,1}(t,u) = L_n(t,u), \tag{5.17}$$

and

$$L_{n,i}(t,u) = \int_u^t L_{n,1}(t,x)\; L_{n,i-1}(x,u)\, dx, \quad i \geq 2. \tag{5.18}$$

This corollary (with notations defined in formulas (5.8), (5.9), (5.12), (5.13)) provides a new exact formula for inversion of the circular Radon transform in circular acquisition geometry. Its advantage compared to all the other known exact inversion formulas is the fact that only part of the Rf data is used. Notice that to reconstruct the function $f(r,\theta)$ in any subset Ω of the disc of its support $D(0,R)$, the inversion

formula in Corollary 11 requires the knowledge of $Rf(\rho, \phi)$ only for $\rho < R - R_0$, where $R_0 = \inf\{|x|,\ x \in \Omega\}$. In medical imaging reducing the radial data redundancy can be essential for increasing the depth and reducing the time of imaging.

We can also remark that the resolvent kernel $H_n(t, u)$ is the same for any functions f and g. Hence in practice one needs to compute it with the desired accuracy only once, and then it can be used with any data set.

In Theorem 10, we require f to be continuous, which guarantees the convergence of the Fourier series (5.2) and (5.3) almost everywhere. If one needs to ensure convergence everywhere, then some additional conditions on f (e.g. bounded variation) should be added in all the theorems.

5.2 Exterior problem

Let us now consider an exterior problem in the circular acquisition geometry, i.e. the Radon data is still collected along circles centered on a circle of radius R, however the unknown function f is supported outside of the disc $D(0, R)$.

Theorem 12. *Let $f(r, \theta)$ be an unknown continuous function supported inside the annulus $A(R, 3R) = \{(r, \theta) : r \in (R, 3R),\ \theta \in [0, 2\pi]\}$. If $Rf(\rho, \phi)$ is known for $\phi \in [0, 2\pi]$ and $\rho \in [0, R_1]$, where $0 < R_1 < 2R$ then $f(r, \theta)$ can be uniquely recovered in $A(R, R + R_1)$.*

Proof.

The argument of the proof of the previous theorem repeats here with minimal changes. The condition $0 < R_1 < 2R$ guarantees that all integration circles $C(\rho, \phi)$ intersect the boundary of the disc $D(0, R)$. Hence equation (5.4) in this case becomes

$$g(\rho, \phi) = \sum_{n=-\infty}^{\infty} 2\, e^{in\phi} \int_R^{R+\rho} \frac{f_n(r)\ r \cos\left[n \arccos\left(\frac{r^2+R^2-\rho^2}{2rR}\right)\right]}{R\sqrt{1 - \left(\frac{\rho^2+R^2-r^2}{2\rho R}\right)^2}}\, dr. \tag{5.19}$$

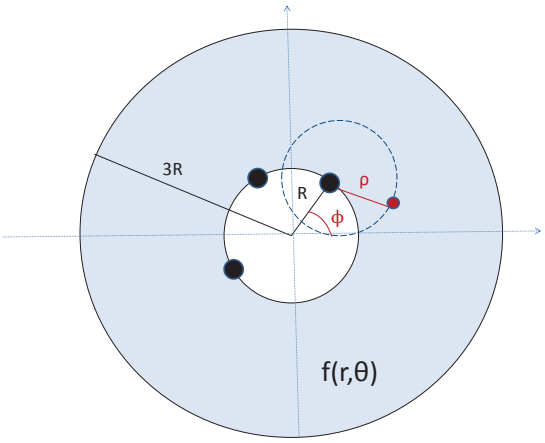

Figure 5.3. The exterior problem.

Then in a similar way, we have

$$g_n(\rho) = 2\int_R^{R+\rho} \frac{f_n(r)\; r\; T_{|n|}\left(\frac{r^2+R^2-\rho^2}{2rR}\right)}{R\sqrt{1-\left(\frac{\rho^2+R^2-r^2}{2\rho R}\right)^2}}\, dr, \tag{5.20}$$

Now making a change of variables $u = r - R$ in the last expression we get

$$g_n(\rho) = \int_0^{\rho} \frac{f_n(R+u)\, 4\rho\,(R+u)\; T_{|n|}\left[\frac{(R+u)^2+R^2-\rho^2}{2R\,(R+u)}\right]}{\sqrt{\rho-u}\sqrt{(u+\rho)(2R+u+\rho)(2R+u-\rho)}}\, du. \tag{5.21}$$

which can be rewritten as

$$g_n(\rho) = \int_0^{\rho} \frac{F_n(u)\, K_n(\rho,u)}{\sqrt{\rho-u}}\, du, \tag{5.22}$$

where

$$F_n(u) = f_n(R+u), \tag{5.23}$$

$$K_n(\rho,u) = \frac{4\rho\,(R+u)\; T_{|n|}\left[\frac{(R+u)^2+R^2-\rho^2}{2R\,(R+u)}\right]}{\sqrt{(u+\rho)(2R+u+\rho)(2R+u-\rho)}}. \tag{5.24}$$

Notice, that if one would allow $\rho > 2R$, then $K_n(\rho,u)$ would become unbounded due to the last multiplier in the denominator. This shows that $3R$ is an accurate upper limit for the outer radius of the annulus in the hypothesis of the theorem.

In analogy with the proof of the previous theorem we get

$$K_n(t,t) = \sqrt{\frac{2t\,(R+t)}{R}} \neq 0.$$

All the other steps literally repeat the proof of Theorem 10.

5.3 Special case

It is easy to note that in some special cases one can combine the results of the previous two theorems to reconstruct a function whose support is located both inside and outside of the circular path $C(R)$ of data acquisition. For example

Theorem 13. *Let f be an unknown continuous function supported inside the disc $D(0,2R)$. Assume also that $f \equiv 0$ in some neighborhood of the circle $C(R)$, and all its Fourier coefficients are even (or odd) with respect to $C(R)$, i.e. $f_n(R+u) = f_n(R-u)$ (or $f_n(R+u) = -f_n(R-u)$) for $\forall u \in [0,R]$. If $Rf(\rho,\phi)$ is known for $\phi \in [0,2\pi]$ and $\rho \in [0,R_1]$, where $0 < R_1 < R$ then $f(r,\theta)$ can be uniquely recovered in $A(R-R_1,\, R+R_1)$.*

Proof. Combining the two previous results, we obtain a Volterra integral equation of the first kind

$$g_n(\rho) = \int_0^\rho \frac{F_n(u)K_n(\rho,u)}{\sqrt{\rho-u}}\,du, \tag{5.25}$$

where

$$F_n(u) = f_n(R+u), \tag{5.26}$$

and

$$K_n(\rho,u) = \tag{5.27}$$

$$\frac{4\rho}{\sqrt{u+\rho}}\left\{\frac{(R+u)\,T_{|n|}\left[\frac{(R+u)^2+R^2-\rho^2}{2R\,(R+u)}\right]}{\sqrt{(2R+u+\rho)(2R+u-\rho)}}\pm\frac{(R-u)\,T_{|n|}\left[\frac{(R-u)^2+R^2-\rho^2}{2R\,(R-u)}\right]}{\sqrt{(2R+\rho-u)(2R-\rho-u)}}\right\}.$$

The rest of the proof is carried out along the same lines as before.

It is interesting to note that the circular Radon transform in the linear acquisition geometry can be uniquely inverted on the class of continuous functions that are even with respect to the linear path of the data acquisition. At the same time all odd functions are mapped to zero by that transform. In our case of circular acquisition geometry, the circular Radon transform can be uniquely inverted on classes of functions with Fourier coefficients that are even with respect to the circular path of data acquisition, as well as with the ones that are odd.

Conclusion: The purpose of this chapter has been to present our new mathematical results on uniqueness and recovery of the image function from radially partial data. To our knowledge, this is the first work to explicitly formulate such inversion formulas in the case of the circular acquisition geometry for both interior and exterior problems. The numerical implementation of these formulas is an important topic for future investigation.

The results are not only interesting as original mathematical discoveries, but can also be useful for applications, e.g. in medical imaging. While it is well established that acoustic tomography in its various forms is a classic example of spherical Radon-based imaging *inside* a spherical/circular (3D/2D) aperture, the case of imaging *outside* a spherical aperture is less described biomedically. Two biomedical imaging methods can currently be modeled in the time domain through spherical transforms of a function exterior to the aperture: transrectal ultrasound (TRUS) [48] and intravascular ultrasound (IVUS) [17]. In both TRUS (Figure 5.5) and IVUS (Figure 5.4), a ultrasound array arranged on the surface of a cylinder is introduced

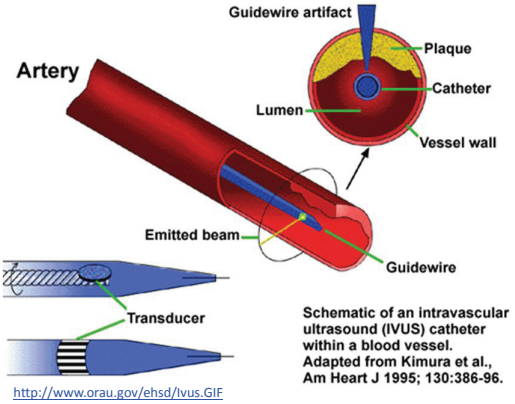

Figure 5.4. Intravascular ultrasound.

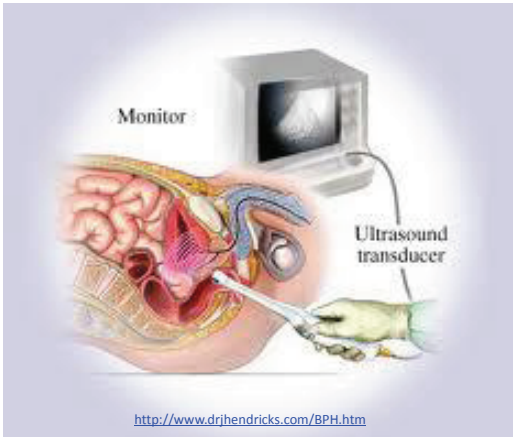

Figure 5.5. Transrectal ultrasound.

into the body with the goal of producing a transverse or axial image. In TRUS, the typical application is imaging of the male prostate, while IVUS is a higher resolution ultrasound technique typically used to evaluate plaques in blood vessels. A less natural setup where the support of the unknown function is located on both sides of the data acquisition path may not be relevant to medical imaging, however it can be applicable in radar and sonar imaging.

CHAPTER 6

APPROXIMATE INVERSION OF ERT: NUMERICAL RESULTS

In circular acquisition geometry, we presented several exact inversion formulas to recover an unknown function from its circular Radon transform. That setup corresponds to the mathematical model of ultrasound reflection tomography in monostatic regime. As it was mentioned before, in bistatic regime the corresponding mathematical model is based on the elliptical Radon transform. Although, S. Mensah and E. Franceschini investigated the inversion of the elliptical Radon transform in [39, 40], this case is still not completely understood. To the best of our knowledge no exact inversion formula is known for the reconstruction from elliptical Radon transform in the circular aperture. Instead, many authors resort to approximate inversion algorithms, such as the recent publication [52] and the work done by T. Quinto and his student H. Levinson to develop novel local reconstruction methods for bistatic radar and ultrasound imaging [36].

In this chapter, we describe an approximate inversion of the elliptical Radon transform when the source and the receiver (the foci of the integration ellipse) are rotating around the origin at a fixed distance from each other, as illustrated in Figure 6.1. We demonstrate the efficiency of the suggested algorithm by presenting a computational implementation of the method on a numerical phantom. We explain how to generate a sample image, collect its integrals over a family of ellipses and then derive a filtered backprojection (FBP) algorithm to reconstruct important features (e.g. boundaries) of the original image.

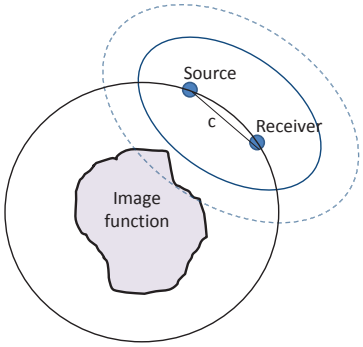

Figure 6.1. Circular acquisition geometry.

6.1 Reconstruction algorithm

Let C designate the circle centered at the origin $(0, 0)$ and of radius R. We consider the case of circular acquisition geometry where the source and the receiver are rotating on the circle C. We also assume that the distance c between the source and the receiver is constant (see Figure 6.1). We parameterize the source and the receiver location by the angle ϕ, where $\phi \in [0, 2\pi)$ is the polar angle of the midpoint (cx, cy) measured from the x-axis. For simplicity, we assume that the centers (cx, cy) are rotating on the unit circle. The Figure 6.2 illustrates the circular acquisition geometry and the center's location at a rotation angle ϕ.

To generate the data, we create a sample image called a phantom. Then we compute its integrals over family of ellipses with foci at the source and the receiver locations. The collected integrals are the values of elliptical Radon transform Rf that we use later in the FBP algorithm to reconstruct the features of the original phantom. Now let us look at each of these steps in a little more detail.

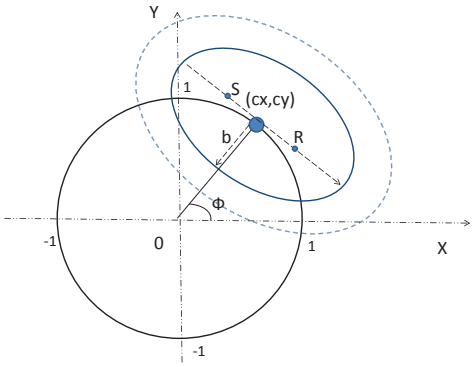

Figure 6.2. Geometric setup of integration.

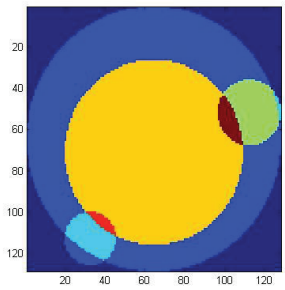

Figure 6.3. Phantom image.

6.1.1 Generation of the phantom image

Numerically, we consider the grid that specifies a pixelated representation of [-1,1] × [-1,1]. The phantom images that we consider are represented by sums of indicator functions of simple objects, like circles and squares. To determine whether a particular pixel lies in the interior of a circle or a square, we look at the center of the pixel. If the center of the pixel lies within a circle/square then we attribute the intensity of the circle/square to the pixel's value. If a pixel is not part of any

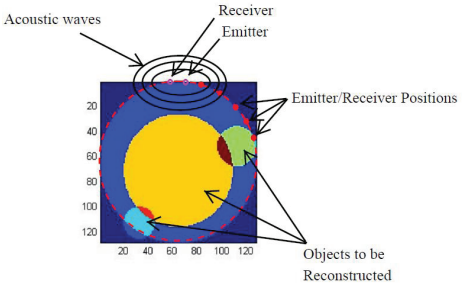

Figure 6.4. Projection data.

circles/squares, its value is 1. In other words, the intensity values of all the pixels in the unit circle define the function $f(x, y)$ as follows:

$$f(x,y) = \begin{cases} I & \text{the center of the pixel inside some of the circles/squares,} \\ 1 & \text{the center of the pixel outside all circles/squares.} \end{cases}$$

where I is equal to the sum of the additive intensity values of all circles/squares that the pixel is a part of.

6.1.2 Computation of the projection data

Once we create the phantom, we need to generate the projection data which is the integrals of the phantom over family of ellipses. As defined in the introduction, we specify the position of the integration ellipse $E(b, \phi)$ by the angle ϕ which is the polar angle of the center of the ellipse (cx, cy) and the semi-minor axis b. Because in practical applications the data is sampled at a finite set of points on the unit circle, we discretize the problem by considering only a finite number of angles ϕ and a finite number of samples of the semi-minor axis b. So we uniformly discretize the data

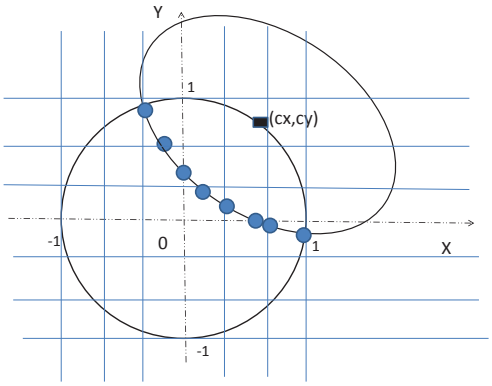

Figure 6.5. Intersection points of an ellipse with the grid.

$[0, 2] \times [0, 2\pi]$ of b and ϕ to N_b and N_ϕ points, respectively. At each point (b^k,ϕ^j), we compute the value of the elliptical Radon transform $Rf(b^k, \phi^j)$:

$$Rf(b^k, \phi^j) := Rf^{k,j} \quad (k, j) \in \{0, ..., N_b\} \times \{0, ..., N_\phi\}.$$

Our appraoch for approximating the integral of the intensity function along any given ellipse $E(b^k, \phi^j)$ is to measure the distance between the neighboring intersection points of the ellipse with vertical and horizontal grid lines and then multiply it by the intensity of the pixel where the points are located.

- *Step 1*

Using $N \times N$ grid that represents [-1,1] $\times$ [-1,1], we compute the intersections of a given ellipse $E(b^k, \phi^j)$ with all vertical and horizontal grid lines located in the unit circle (Figure 6.5).

- *Step 2*

Then by applying the equation (6.1), we estimate the polar angle α between the vector v (connecting the intersection point and (cx, cy)) and the unit vector $\hat{i}$ of the x-axis (Figure 6.6).

$$\alpha = \pm \arccos\left(\frac{v \cdot \hat{i}}{\|v\|\|\hat{i}\|}\right). \tag{6.1}$$

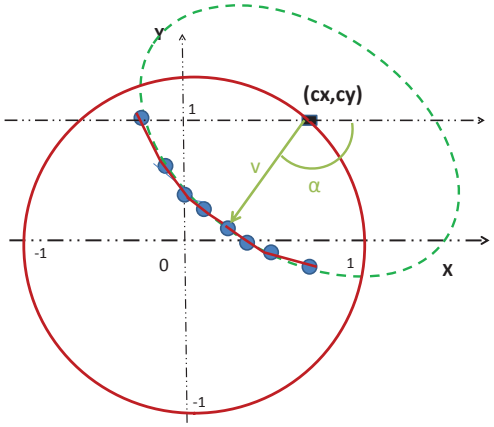

Figure 6.6. The vector v and the angle α.

A major advantage of computing the values of α for the forward problem is that now one can sort the intersection points into the order in which they occur along the ellipse clockwise starting at the west pole. Then, we can easily measure the distance between any consecutive points (see Figure 6.6).

- *Step 3*

Once we measure the distance between any two intersection points, we multiply it by the intensity of the pixel where the points are located. The obtained value is the approximation of the integral of the intensity function along the arc joining these points. This operation is repeated for each pair of intersection points and the resulting values are summed to form an approximate integral of the phantom along the ellipse $E(b^k, \phi^j)$.

We repeat the same process for all the ellipses $E(b^k, \phi^j)$ with $(k, j) \in \{0, ..., N_b\} \times \{0, ..., N_\phi\}$. The result is the discrete value of the elliptical Radon transform Rf that we will use in the FBP algorithm to reconstruct the phantom.

6.1.3 Reconstruction of the phantom image

In the following reconstruction approach, we simply use an approximate FBP algorithm similar to the reconstruction algorithm for the classical Radon transform described in chapter 4. The FBP algorithm involves two steps: (1) each of the projections in the Radon transform is filtered then (2) backprojected to reconstruct the original image.

- *Step 1*

Here we implement a similar procedure for the elliptical Radon transform using the coordinates (b, ϕ) that are analogs of (ρ, ϕ) in the classical Radon transform. Let us recall the filter F defined in the equation (4.9) and represented as follows:

$$Ff(w) = \int_{-\infty}^{\infty} \hat{f}(b)\, e^{ibw}\, |b|\, db. \tag{6.2}$$

This equation represents a filtering operation that can be expressed as a composition of two simpler operations: differentiation and the Hilbert transform. In fact, the Fourier transform of the derivative of the function f is equal to the Fourier transform of f multiplied by ib

$$\widehat{\partial_t f(b)} = (i\, b)\, \hat{g}(b).$$

So to use differentiation and account for the difference between b and $|b|$, we define another operator called the Hilbert transform

$$Hf(x) = \frac{1}{\pi} \int_{-\infty}^{\infty} \frac{f(y)}{x - y}\, dy.$$

This implies that

$$\widehat{Hf(w)} = (-i\, \mathrm{sgn}(w))\, \hat{f}(w),$$

where

$$\operatorname{sgn}(w) = \begin{cases} 1 & \text{if } w > 0, \\ 0 & \text{if } w = 0, \\ -1 & \text{if } w < 0. \end{cases}$$

By the above equation (6.2), the filtering operation consists of differentiating the function with respect to the semi-minor axis b and then applying the Hilbert transform.

- *Step 2*

The next main reconstruction step involves a process known as backprojection which takes the data from the filtered projections and projects it back along the same ellipses from where the data was collected. So to compute the function at any given point (x, y) in the unit circle, we average the filtered data over all ellipses passing through that point.

$$f(x, y) = \int_0^{2\pi} F(b(\phi), \phi)\, d\phi,$$

This equation adds the resulting filtered projections $F(b, \phi)$ for different angles ϕ to form the estimate of $f(x, y)$. A common discrete approximation to the integral is obtained by:

$$f(x_n, y_n) = \triangle\phi \sum_{m=0}^{N_\phi} F(b(\phi_m), \phi_m),$$

where $\triangle\phi = \frac{2\pi}{N_\phi}$. N_ϕ is the number of angles ϕ for which the projections $Rf(b, \phi)$ are known. It should be noted here that the value of $b(\phi_m)$ may not correspond exactly to a value of m for the filtered projections that we calculated in the previous step. In order to be able to compute $f(x_n, y_n)$ one must then interpolate $b(\phi_m)$.

To implement the algorithm, we sampled the filter and discretized the backprojection operation. The important steps of the approximate FBP are outlined below:

1. Perform the FFT of the projection data for each angle ϕ.
2. Multiply the result with response function in the frequency domain.
3. Perform the IFFT of the result. This provides us the filtered projections in the discrete domain at the various angles ϕ.
4. Sum the filtered projections. The result $f_{FBP}(x, y)$ is an approximation of $f(x, y)$.

6.2 Numerical results

In this section, we present some numerical results of our inversion algorithm for different phantoms to demonstrate its performance. The data is collected from detectors located on the unit circle. Therefore, the region of reconstruction is the unit circle centered at the origin.

In a recent work [8], the authors studied microlocal properties of the ERT in the circular acquisition geometry, and showed that the composition of the ERT with its adjoint (the backprojection operator) is an elliptic pseudo-differential operator. This means that the approximate inversion algorithm based on the backprojection correctly reconstructs the singularities of the object and does not add any additional singularities. Our numerical experiments below validate this result, and present an effective implementation of the technique. Similar algorithms have been recently by other authors, including [36], and [52].

In the results in Figure 6.7, the resolution is 64×64. The angles ϕ of the center locations were uniformly discretized to $N_\phi = 64$ points between 0 and 2π. The semi-minor axis of the integration ellipses were uniformly discretized to $N_b = 64$ points between 0 and 2.

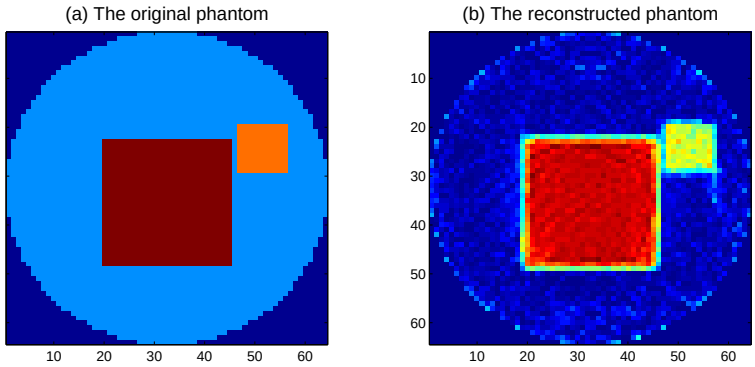

Figure 6.7. Numerical results for 2 squares using $N = 64$.

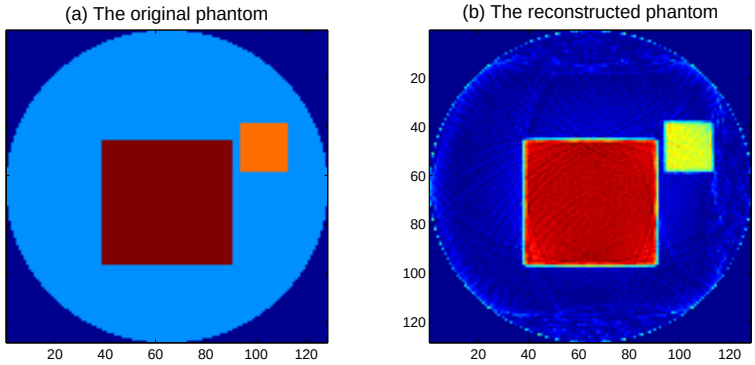

Figure 6.8. Numerical results for 2 squares using $N = 128$.

Next, we increase the number of discretization. We present new set of results with resolution 128×128. As one might expect, we achieve a better reconstruction when we decrease the sampling interval (see Figure 6.8). Additionally, the noisy images in Figure 6.7 appear to be smoothed as compared to the Figure 6.8.

We tested the algorithm on a phantom containing 3 circles (Figure 6.10), the parameters of which are given in Table 6.1. We enumerate the circles from 1 to 3 starting with the circle with highest center.

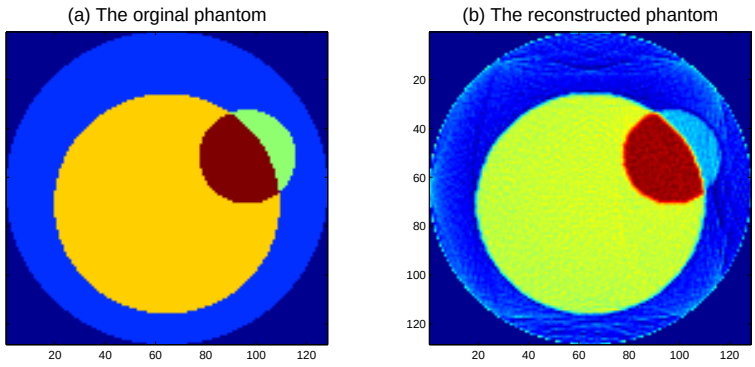

Figure 6.9. Numerical results for a phantom with 2 circles.

Table 6.1. Parameters for the Fig. 6.10

Circle	Coordinates of the center (x, y)	radius	intensity
1	(0.6,0.4)	0.2	2
2	(0.0,-0.1)	0.5	3
3	(-0.5,-0.5)	0.1	1

We tested the algorithm on a phantom containing 3 squares (Figure 6.11), the parameters of which are given in Table 6.2. We enumerate the squares from 1 to 3 starting with the square with highest center.

Table 6.2. Parameters for the Fig. 6.11

Square	Coordinates of the center (x, y)	length	intensity
1	(0.4,0.5)	0.2	1
2	(0.6,0.25)	0.3	2
3	(0.0,-0.1)	0.8	3

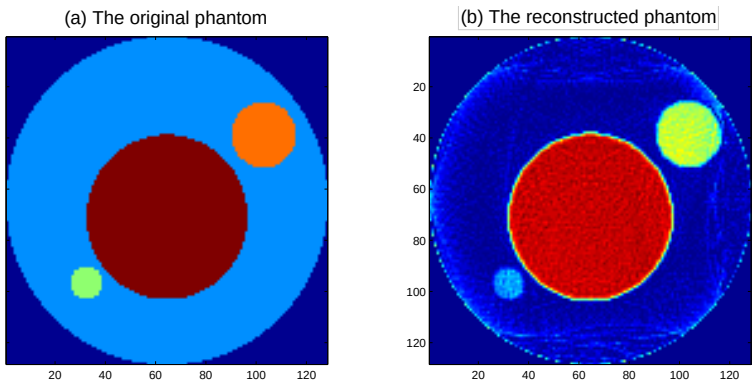

Figure 6.10. Numerical results for a phantom with 3 circles.

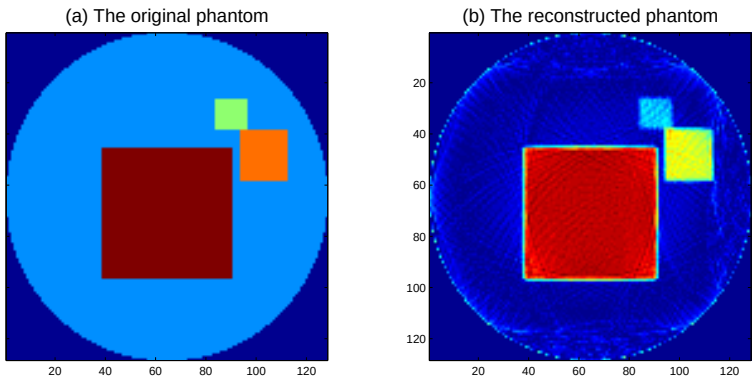

Figure 6.11. Numerical results for a phantom with 3 squares.

CHAPTER 7

DIRECTIONS FOR FURTHER WORK

The new mathematical results presented in this dissertation have the potential to be generalized to higher dimensions using spherical harmonics and Gegenbauer polynomials [1], similarly to the generalization of Cormack's original inversion formula (e.g. see [22, 41]). In addition, possible future work can be done to extend our approach to other transforms of Radon type e.g. the elliptical Radon transform.

Another perspective for future work is to derive an accurate and efficient numerical implementation of our new inversion formulas for both interior and exterior problems when the Radon transform is known for only a part of all possible radii.

The algorithm described in chapter 6 used an approximate inversion formula to reconstruct the image function from its integrals along ellipses rotating around the origin. A direction for future work is to derive an exact inversion formula for the elliptical Radon transform in 2D and 3D cases, and then implement it numerically. Also the uniqueness problem for the elliptical Radon transform still remains unresolved in the case of circular and spherical aperture. These open problems may be relevant to several imaging modalities and practical applications working in the near field zone or with bistatic measurements.

CHAPTER 8

CONCLUSION

In the last decade, there has been a substantial spike of interest towards the problem of reconstructing a function from its circular Radon transform mainly due to its connection with some mathematical models of advanced imaging modalities. In circular acquisition geometry there are various inversion formulas when the circular Radon transform Rf is known for circles of all possible radii. However, to the best of our knowledge no exact formula is known for the case when Rf is available for only a part of all possible radii, or when the support of the function f is outside the circle.

In this dissertation, we presented our new results about the existence and uniqueness of the representation of a function by its circular Radon transform with radially partial data. A new inversion formula is described in the case of the circular acquisition geometry for both interior and exterior problems when the Radon transform is known for only a part of all possible radii. We also investigated a reconstruction algorithm applicable in the case of elliptical Radon transform based on an approximate backprojection formula.

The results are not only interesting as original mathematical discoveries, but can also open new frontiers in the field of imaging.

REFERENCES

[1] M. Abramowitz and I. A. Stegun, *Handbook of Mathematical Functions with Formulas, Graphs, and Mathematical Tables*, Dover Publications, New York, 1972.

[2] M. L. Agranovsky, C. A. Berenstein and P. Kuchment, "Approximation by spherical waves in L^p-spaces," *J. Geom. Anal.*, **6** (1996), 365–383.

[3] M. L. Agranovsky, P. Kuchment and L. Kunyansky, "On reconstruction formulas and algorithms for the thermoacoustic and photoacoustic tomography," in *Photoacoustic imaging and spectroscopy, ed. L.-H. Wang*, CRC Press, 2009.

[4] M. L. Agranovsky, P. Kuchment and E. T. Quinto, "Range descriptions for the spherical mean Radon transform," *J. Funct. Anal.*, **248** (2007), 344-386.

[5] M. L. Agranovsky and P. Kuchment, "Uniquness of reconstruction and an inversion procedure for thermoacoustic and photoacoustic tomography with variable sound speed," *Inverse Problems*, **23** (2007), 2102-2007.

[6] M. L. Agranovsky and E. T. Quinto, "Injectivity sets for the Radon transform over circles and complete systems of radial functions," *J. Funct. Anal.*, **139** (1996), 383–413.

[7] G. Ambartsoumian, R. Gouia-Zarrad and M. Lewis, "Inversion of the circular Radon transform on an annulus," *Inverse Problems*, **26** (2010), 105015.

[8] G. Ambartsoumian, V. Krishnan and E. T. Quinto, "The microlocal analysis of the ultrasound operator with circular source and receiver trajectory," *preprint.*

[9] G. Ambartsoumian and P. Kuchment, "On the injectivity of the circular Radon transform," *Inverse Problems*, **21** (2005), 473.

[10] G. Ambartsoumian and P. Kuchment, "A range description for the planar circular Radon transform," *SIAM J. Math. Anal.*, **38** (2006), 681–692.

[11] M. Anastasio, J. Zhang, E. Sidky, Y. Zou, D. Xia and X. Pan, "Feasibility of half-data image reconstruction in 3D reflectivity tomography with a spherical aperture," *IEEE Trans. Med. Imag.*, **24** (2005), 1100–12.

[12] M. Anastasio, J. Zhang, X. Pan, Y. Zou, G. Ku and L. V. Wang, "Half-time image reconstruction in thermoacoustic tomography," *IEEE Trans. Med. Imag.*, **24** (2005), 199–210.

[13] M. Anastasio, X. Pan and Y. Zou, "Data Redundancy and Reduced-Scan Reconstruction in Reflectivity Tomography," *IEEE Transactions on Image Processing*, **12** (2003), 784–95.

[14] L.-E. Andersson, "On the determination of a function from spherical averages," *SIAM J. Math. Anal.*, **19** (1988), 214–232.

[15] M. Born and E. Wolf, *Principles of optics: electromagnetic theory of propagation, interference and diffraction of light*, Oxford, New York, Pergamon Press, 1965.

[16] M. Cheney, "Tomography prolems arising in Synthetic Aperture Radar," in *Radon Transforms and Tomography,* ed. *E.T. Quinto, L. Ehrenpreis, A. Faridani, F. Gonzalez, E. Grinberg*, American Math. Soc., Providence, RI, 2001.

[17] R. Cobbold, *Foundations of Biomedical Ultrasound*, Oxford Univ. Press, 2007.

[18] J. Coker and A. Tewfik, "Multistatic SAR image reconstruction based on an elliptical-geometry Radon transform," *2007 International Waveform Diversity and Design Conference*, 204–208, IEEE Conference Proceedings, 2007.

[19] A. Cormack, "Representation of a function by its line integrals, with some radiological applications," *J. Appl. Phys.* **34** (1963), 2722–27.

[20] A. Cormack, "Representation of a function by its line integrals, with some radiological applications II," *J. Appl. Phys.* **35** (1964), 2908–12.

[21] R. Courant and D. Hilbert, *Methods of Mathematical Physics*, Vol.2, Wiley, New York, 1989.

[22] S. Deans, "Gegenbauer transforms via the Radon transform," *SIAM J. Math. Anal.*, **10** (1979), 577–85.

[23] S. Deans, *The Radon transform and some of its applications* , Dover Publications, New York, 1993.

[24] L. Ehrenpreis, *The Universality of the Radon Transform*, Oxford Univ. Press, New York, 2003.

[25] C. Epstein, *Introduction to the mathematics of medical imaging*, SIAM, Philadelphia, 2003.

[26] J. A. Fawcett, "Inversion of n-dimensional spherical averages," *SIAM J. Appl. Math.*, **45** (1985), 336–341.

[27] D. Finch, M. Haltmeier and Rakesh, "Inversion of spherical means and the wave equation in even dimension," *SIAM J. Appl. Math*, **68** (2007), 392–412.

[28] D. Finch and Rakesh, "The spherical mean value operator with centers on a sphere," *Inverse Problems*, **23** (2007), s37–s49.

[29] D. Finch and Rakesh, "The range of the spherical mean value operator for functions supported in a ball," *Inverse Problems*, **22** (2006), 923–938.

[30] D. Finch, Rakesh and S. K. Patch, "Determining a function from its mean values over a family of spheres," *SIAM J. Math. Anal.*, **35** (2004), 1213–1240.

[31] I. Gelfand and G. Shilov, *Generalized Functions*, Vol. 1, Academic, New York, 1964.

[32] S. Helgason, *The Radon Transform*, Birkhäuser, Basel, 1980.

[33] A. C. Kak and M. Slaney, *Principles of Computerized Tomographic Imaging*, IEEE Press, New York, 1988.

[34] P. Kuchment and L. Kunyansky, "A Survey in Mathematics for Industry: Mathematics of thermoacoustic tomography," *European J. Appl. Math.*, **19** (2008), 191–224.

[35] L. Kunyansky, "Explicit inversion formulas for the spherical mean Radon transform," *Inverse Problems*, **23** (2007), 373–383.

[36] H. Levinson, "Reconstruction Algorithms for Bistatic Radar and Ultrasound Imaging," *BS thesis*, (2011).

[37] V. Ya. Lin and A. Pinkus, "Fundamentality of ridge functions," *J. Approx. Theory*, **75** (1993), 295–311.

[38] A. K. Louis and E. T. Quinto, "Local tomographic methods in Sonar," in *Surveys on Solution Methods for Inverse Problems*, 147–154, Springer, Vienna, 2000.

[39] S. Mensah and E. Franceschini, "Near-field ultrasound tomography," *J. Acoust. Soc. Am*, **121** (2007), 1423–1433.

[40] S. Mensah, E. Franceschini and M.-C. Pauzin, "Ultrasound mammography," *Nuclear Instruments and Methods in Physics Research*, Section A, **571** (2007), 52–55.

[41] D. Ludwig, "The Radon transform on Euclidean space," *Comm. Pure App. Math.*, **19** (1966), 41–81.

[42] F. Natterer, *The Mathematics of Computerized Tomography*, Wiley, New York, 1986.

[43] F. Natterer and F. Wübbeling, *Mathematical Methods in Image Reconstruction*, Monographs on Mathematical Modeling and Computation v. 5, SIAM, Philadelphia, PA, 2001.

[44] M. Nessibi, L. Rachdi and K. Trimeche, "Ranges and inversion formulas for the spherical mean operator and its dual," *J. Mat. Anal. Appl.*, **196** (1995), 861–884.

[45] S. J. Norton, "Reconstruction of a reflectivity field fro line integrals over circular paths," *J. Acoust. Soc. Am.*, **67** (1980), 853–863.

[46] S. J. Norton, "Reconstruction of a two-dimensional reflecting medium over a circular domain: Exact Solution," *J. Acoust. Soc. Am.*, **67** (1980), 1266–1273.

[47] S. J. Norton and M. Linzer, "Ultrasonic reflectivity imaging in three dimensions: exact inverse scattering solutions for plane, cylindrical, and spherical apertures," *IEEE Trans. Biomed. Eng.*, **28** (1981), 202–220.

[48] U. Patel and D. Rickards, *Handbook of Transrectal Ultrasound and Biopsy of the Prostate*, Taylor & Francis, 2002.

[49] A. Polyanin and A. Manzhirov, *Handbook of Integral Equations*, Boca Raton: CRC Press, 1998.

[50] T. Rivlin, *Chebyshev Polynomials : From Approximation Theory to Algebra and Number Theory*, John Wiley & Sons, 1990.

[51] F. Tricomi, *Integral Equations*, Dover Publications, New York, 1983.

[52] R. Vaidyanathan, M. Lewis, G. Ambartsoumian and T. Aktosun, "Reconstruction algorithms for interior and exterior spherical Radon transform-based ultrasound imaging," *Proceedings of SPIE*, **7265** (2009), 72651I, 1–8.

[53] V. Volterra, *Theory of Functionals and of Integral and Integro-Differential Equations*, Dover Publications, New York, 2005.

[54] M. Xu and L. Wang, "Universal Back-projection algorithm for photoacoustic computed tomography," *The American Physical Society* , **71** (2005), 016706.

[55] M. Xu and L. Wang, "Photoacoustic imaging in biomedecine," *Review of scientific instruments*, **77** (2006), 041101.

[56] Y. Xu, L. Wang, G. Ambartsoumian and P. Kuchment, "Reconstructions in limited view thermoacoustic tomography," *Medical Physics*, **31** (2004), 724–733.

BIOGRAPHICAL STATEMENT

Rim Gouia was born in Tunisia in 1979. After an excellent A-Level/ baccalaureate degree, she moved to Paris to pursue the prestigious Classes Preparatoires and earn a M.S. in Engineering in 2004 from Ecole Centrale Paris, France. Then she worked for two major corporate houses: Bougues-Construction in France and XTO Energy (currently Exxon Mobile) in USA, before deciding to return to academia and pursue a Ph.D. in Applied Mathematics. Shortly after joining the University of Texas at Arlington (UTA) in 2007, she became a research assistant to Dr. Gaik Ambartsoumian and joined a multidisciplinary research team supported by the US Department of Defense aiming at improving Ultrasound Imaging for cancer screening. She specializes in integral geometry and in particular the mathematical problems of Radon transform applied to advanced imaging. In 2010, she published a paper in the journal *Inverse Problems* titled "Inversion of the circular Radon transform on an annulus". Since then she became a reviewer in the same journal and was invited to several international conferences and workshops.

She has also taught different mathematics classes at various colleges in the US. With her academic background and her multidisciplinary career as engineer and mathematician, she strives to shed some light on the elegance and beauty of mathematics by connecting its conceptual world to solving real-life problems.

Based on her academic achievement and her dedication, the UTA Department of Mathematics selected her as the outstanding student of the year 2010-2011 awarding her the *Stephen R. Bernfeld Memorial Scholarship*.